



HAL
open science

Origin of negative Cerium anomalies in subduction-related volcanic samples: constraints from Ce and Nd isotopes

Nina Bellot-Coignus, Maud Boyet, Régis Doucelance, Pierre Bonnand, Ivan Savov, Terry Plank, Tim Elliott

► **To cite this version:**

Nina Bellot-Coignus, Maud Boyet, Régis Doucelance, Pierre Bonnand, Ivan Savov, et al.. Origin of negative Cerium anomalies in subduction-related volcanic samples: constraints from Ce and Nd isotopes. *Chemical Geology*, 2018, 500, pp.46-63. 10.1016/j.chemgeo.2018.09.006 . hal-02110867

HAL Id: hal-02110867

<https://uca.hal.science/hal-02110867v1>

Submitted on 25 Apr 2019

HAL is a multi-disciplinary open access archive for the deposit and dissemination of scientific research documents, whether they are published or not. The documents may come from teaching and research institutions in France or abroad, or from public or private research centers.

L'archive ouverte pluridisciplinaire **HAL**, est destinée au dépôt et à la diffusion de documents scientifiques de niveau recherche, publiés ou non, émanant des établissements d'enseignement et de recherche français ou étrangers, des laboratoires publics ou privés.

1 **Origin of negative Cerium anomalies in subduction-related**
2 **volcanic samples: constraints from Ce and Nd isotopes**

3
4
5
6
7
8
9
10 *Nina Bellot^a, Maud Boyet^a, Régis Doucelance^a, Pierre Bonnand^a,*
11
12 *Ivan P. Savov^b, Terry Plank^c, Tim Elliott^d*

13
14
15
16
17
18 ^a Université Clermont Auvergne, CNRS, IRD, OPGC, Laboratoire Magmas et Volcans, F-
19 63000 Clermont-Ferrand, France.

20
21
22 ^b *School of Earth and Environment, Institute of Geophysics and Tectonics, University of*
23 *Leeds, Leeds LS2 9JT, UK.*

24
25
26 ^c *Lamont-Doherty Earth Observatory of Columbia University, 61 Route 9W, Palisades, New*
27 *York 10964, USA.*

28
29
30 ^d *Bristol Isotope Group, School of Earth Sciences, University of Bristol, Wills Memorial*
31 *Building, Queen's Road, Bristol BS8 1RJ, UK.*

32
33
34
35
36 **Corresponding author:** maud.boyet@uca.fr

37
38 nina.bellot@gmail.com / r.doucelance@opgc.fr / pierre.bonnand@uca.fr/

39
40 i.savov@see.leeds.ac.uk / tplank@ldeo.columbia.edu / tim.elliott@bristol.ac.uk

41
42
43
44 Main text: 8952 words (without abstract, references, table and figure captions)

45
46 Figures: 11

47
48 Tables: 3

49
50 Supplementary files: 7

51
52
53
54 **ABSTRACT**

55
56 Negative Cerium (Ce) anomalies are observed in chondrite-normalized rare earth element
57 patterns from various volcanic arc suites. These anomalies are well defined in volcanic rocks

29 from the Mariana arc and have been interpreted as the result of addition of subducted
30 sediments to the arc magma sources. This study combines $^{143}\text{Nd}/^{144}\text{Nd}$ and $^{138}\text{Ce}/^{142}\text{Ce}$
31 isotope measurements in Mariana volcanic rocks that have Ce anomalies ranging from 0.97
32 to 0.90. The dataset includes sediments sampled immediately before subduction at the
33 Mariana Trench (Sites 801 and 802 of ODP Leg 129) and primitive basalts from the Southern
34 Mariana Trough (back-arc basin). Binary mixing models between the local depleted mantle
35 and an enriched end-member using both types of sediment (biosiliceous and volcanoclastic)
36 found in the sedimentary column in front of the arc are calculated. Marianas arc lavas have
37 Ce and Nd isotopic compositions that require less than 2.5% of a sediment component
38 derived from the volcanoclastics. With this proportion of sediment, most of the Ce/Ce* range
39 measured in lavas is reproduced. Thus, this study confirms that the origin of the Ce
40 anomalies in the Mariana arc magmas can be principally attributed to recycling of trench
41 sediments through active subduction. The participation of a component derived from
42 biosiliceous sediments does not explain the Ce-Nd isotope composition of the lavas because
43 the involved proportion is too high (up to 8%) in comparison to results obtained from other
44 geochemical proxys. Using this end-member, the modeled Ce anomalies are also too high
45 (0.91-0.84) in comparison to those measured in lavas. Various processes and conditions are
46 able to generate Ce anomalies: oxygen fugacity, residual mineral phases, partial melting,
47 fractional crystallization and tropical weathering. Their influence in the case of Mariana
48 volcanic arc magmas seems to be very limited but partial melting effect may explain the
49 lowest measured Ce/Ce* values. Magmatic processes cannot be definitely ruled out in
50 producing Ce anomalies in other arc system environments. Additional experimental data,
51 however, are needed for a better understanding of the behavior of cerium relative to its
52 neighboring elements. Also, this study highlights the importance of using local depleted
53 mantle and sediments to model the isotopic compositions of arc lavas.

54
55

56 **Highlights:**

- 57 • Origin of negative Ce anomalies in Mariana arc magmas.

- 1
2
3
4
5
6
7
8
9
10
11
12
13
14
15
16
17
18
19
20
21
22
23
24
25
26
27
28
29
30
31
32
33
34
35
36
37
38
39
40
41
42
43
44
45
46
47
48
49
50
51
52
53
54
55
56
57
58
59
60
61
62
- Coupled $^{138}\text{Ce}/^{142}\text{Ce}$ and $^{143}\text{Nd}/^{144}\text{Nd}$ isotope measurements in Mariana arc magmas, sediments and back-arc basalts.
 - Ce-Nd isotopic binary mixing models coupled with Ce/Ce^* prove that volcanoclastic sediments control the Ce/Ce^* in Mariana lavas.

63 **Keyword:** Ce anomalies, $^{138}\text{Ce}/^{142}\text{Ce}$, sediment recycling, Mariana volcanic arc, Rare Earth
64 Elements.

67 1. Introduction

68
69 Arc magmas record chemical signatures associated with subduction processes. The
70 subducted slab inventory is made up of variously altered and different in age subducted
71 oceanic crust and its sedimentary cover. The sediments are diverse in type and origin
72 depending on the age of the subducting plate, proximity to a continent, and the presence or
73 absence of an accretionary prism (Plank and Langmuir, 1998a; von Huene and Scholl, 1991).
74 Cerium anomalies have been measured in arc rocks from different localities, particularly the
75 New Britain, Mariana, Tonga, Central America and the Lesser Antilles (Carr et al., 1990;
76 Dixon and Batiza, 1979; Ewart et al., 1973; Jakes and Gill, 1970; White and Patchett, 1984).
77 A negative Ce anomaly means that the Ce concentration normalized to the chondritic value is
78 lower than the value interpolated from the two neighboring Rare Earth Elements (REE)
79 Lanthanum (La) and Praseodymium (Pr). The origin of negative Ce anomalies in arc settings
80 has been attributed to the addition of sedimentary component to the arc magma source
81 (Dixon and Batiza, 1979; Elliott et al., 1997; Hole et al., 1984; Woodhead, 1989). Cerium is
82 the only REE that exists in either 3^+ or 4^+ oxidation states and in nature Ce fractionations are
83 related to the changes of the redox conditions. The short residence time of Ce^{4+} in seawater
84 relative to the trivalent Ce^{3+} ions explains the large negative Ce anomaly in the seawater REE
85 pattern (Elderfield and Greaves, 1982). Fe-Mn crusts and MnO clays preferentially scavenge
86 Ce^{4+} relative to other REE^{3+} and thus have positive Ce anomalies (Amakawa, 1991; Bau et
87 al., 2014). Conversely, negative Ce anomalies are generally identified in authigenic clays,

1
2
3
4
5
6
7
8
9
10
11
12
13
14
15
16
17
18
19
20
21
22
23
24
25
26
27
28
29
30
31
32
33
34
35
36
37
38
39
40
41
42
43
44
45
46
47
48
49
50
51
52
53
54
55
56
57
58
59
60
61
62
63
64
65

88 hydrothermal sediments, nannofossil ooze, or fish debris (Moiroud et al., 2015; Picard et al.,
89 2002; Plank and Langmuir, 1998). The geochemical composition of subducting sediments is
90 now fairly well known globally (Plank, 2013). However, the average “global subducting
91 sediment” reservoir (GLOSS, see Plank and Langmuir (1998) and Plank (2013)) does not
92 show significant Ce anomaly with Ce/Ce* values of 0.97 and 1.02 for GLOSS I and GLOSS II,
93 respectively. The majority of the mean trench sedimentary piles in individual subduction
94 zones used for the GLOSS reservoir calculation have negative Ce/Ce* values (57% of them
95 based on the weighted mean composition of each pile). The lack of anomaly in GLOSS
96 reflects the dominance of volcanic ashes and turbidites in some trench sediments that
97 represent large masses in the total budget, which are deposited too quickly to fractionate Ce
98 from other REE.

100 The ^{138}La - ^{138}Ce isotope systematics ($T_{1/2} = 292.5$ Ga; Tanimizu, 2000) is an interesting
101 tool to trace the recycling of sediments in subduction zones since material characterized by
102 Ce anomalies have fractionated La/Ce ratios and then will develop by radiogenic ingrowth
103 different $^{138}\text{Ce}/^{142}\text{Ce}$ ratios. Calculations show that significant deviations of the $^{138}\text{Ce}/^{142}\text{Ce}$
104 ratio from the chondritic reference can be generated in less than 100 Ma in sediments
105 characterized by highly fractionated La/Ce ratios (3-8) as those measured in seawater (see
106 Figure 1 in Bellot et al., 2015). Thus, combining the ^{138}La - ^{138}Ce and ^{147}Sm - ^{143}Nd systematics
107 in magmatic arc samples may offer a unique opportunity to better characterize the nature of
108 the sediments involved in the magma genesis because these sediments are characterized by
109 different REE patterns and evolve to distinct $^{138}\text{Ce}/^{142}\text{Ce}$ and $^{143}\text{Nd}/^{144}\text{Nd}$ isotopic signatures.
110 The Mariana arc is an ideal test site because this arc-basin subduction system is of intra-
111 oceanic type (located >2000 km away from continents) experiencing no terrigenous (crustal)
112 inputs to its trench sediments. Moreover, the plate entering into subduction is one of the
113 oldest at the Earth’s surface (~ 170 Ma old; Bartolini and Larson, 2001; Koppers et al., 2003).
114 On average the sedimentary material at the Mariana Trench is characterized by a large
115 negative Ce/Ce* values of 0.73 (Plank, 2013) and sediments drilled on the fore-arc area show
116 ages up to 170 Ma (Karpoff, 1992). During this period the subducted material will develop a
117 radiogenic $^{138}\text{Ce}/^{142}\text{Ce}$ signature. The increase is +0.7 epsilon unit considering the average

118 La/Ce ratio estimated for the bulk sedimentary column whereas the excess is +1.5 ϵ -unit for
119 sediments characterized by the strongest La/Ce ratios (>0.85). Finally the Mariana Islands
120 have been extensively studied with the aim of characterizing the nature of outfluxes
121 originating from the subducting slab (e.g. Chauvel et al., 2009; Elliott et al., 1997; Freymuth et
122 al., 2015; Gribble et al., 1998; Hole et al., 1984; Ishikawa and Nakamura, 1994; Martindale et
123 al., 2013; Meijer, 1976; Meijer and Reagan, 1981; Moriguti and Nakamura, 1998; Ribeiro et
124 al., 2015; Savov et al., 2005, 2007; Snyder et al., 2004; Stolper and Newman, 1994; Straub,
125 2003; Tollstrup and Gill, 2005; Wade et al., 2005; Woodhead et al., 2012; Woodhead, 1989,
126 1988; Woodhead and Fraser, 1985). The correlation observed between Ce/Ce* and several
127 other proxys (i.e. Ba/La, $^{143}\text{Nd}/^{144}\text{Nd}$) confirms that the negative cerium anomalies measured
128 in Marianna lavas are likely to be inherited from the sedimentary component rather than
129 reflecting the process by which it was transferred (Elliott et al., 1997). Here we present La-Ce
130 and new Sm-Nd isotope measurements in arc lavas coming from the Mariana Islands (Central
131 Island province), in sediments sampled in front of the subduction trench, and in basalts from
132 the back-arc area. We discuss the origin of negative cerium anomalies with respect to
133 $^{138}\text{Ce}/^{142}\text{Ce}$ and $^{143}\text{Nd}/^{144}\text{Nd}$ isotope ratios and then extend our conclusions to the whole
134 database of samples collected in the context of subduction zone for which combined Ce and
135 Nd isotope measurements are available.

136
137

138 2. Geological settings and sample selection

139

140 The Mariana volcanic arc represents the southern segment of the Izu-Bonin-Mariana (IBM)
141 arc-basin system, which results from the > 50 Ma of subduction of the Pacific plate under the
142 Philippine Sea plate. The subducting Pacific plate is Jurassic (~ 170 Ma old; Bartolini and
143 Larson, 2001; Koppers et al., 2003), making it the oldest subducted oceanic slab. Its
144 subduction rate is relatively slow (~4 cm/yr) (Seno, 1977; Stern et al., 2003). The IBM
145 volcanic arc is 2800 km long and extends from Mt. Fuji volcano on the Japanese peninsula to
146 the island of Guam in the south. The Mariana arc can be divided into three well-defined
147 zones: the fore-arc, the magmatic front and the back-arc basin or the Mariana Trough (Figure

1
2
3
4
5
6
7
8
9
10
11
12
13
14
15
16
17
18
19
20
21
22
23
24
25
26
27
28
29
30
31
32
33
34
35
36
37
38
39
40
41
42
43
44
45
46
47
48
49
50
51
52
53
54
55
56
57
58
59
60
61
62
63
64
65

148 1). The Mariana fore-arc corresponds to the area between the trench and the magmatic arc
149 front and is characterized by lack of accretionary sedimentary prism i.e. all sediments and
150 underlying Pacific oceanic crust are effectively subducted. The magmatic front of the Mariana
151 arc includes around 40 active volcanoes (Pearce et al., 2005), many of which are currently
152 submerged. The volcanic activity over the last two centuries has been sub-aerial in the central
153 part and underwater in the northern and southern arc segments. The western segment of the
154 arc forms the actively spreading back-arc: the Mariana Trough. The opening of this back-arc
155 basin is related to intra-arc rifting due to tectonic forces associated with the NW subduction of
156 the Pacific plate and the rotation and spreading within the Philippine Sea plate (Stern et al.,
157 2003). The back-arc converges in the south and north with the magmatic arc front (see Figure
158 1). The maximum back-arc basin width is 100 km in the center (Pearce et al., 2005). The
159 magmatic activity in the back-arc results from adiabatic decompression melting due to
160 seafloor extension combined with fluid mediated melting (Kelley et al., 2010). The back-arc
161 basalt compositions are either MORB-type or arc-type basalts, depending on the proportion of
162 fluids coming from the subducted slab that have been introduced into the otherwise highly
163 depleted sub-arc mantle underneath (Gribble et al., 1996; Pearce et al., 2005; Savov et al.,
164 2005, 2007; Stolper and Newman, 1994; Taylor and Martinez, 2003; Volpe et al., 1987;
165 Woodhead et al., 1993).

166
167 Twelve fresh basaltic to basaltic-andesite samples from the Mariana central island arc
168 volcanic province have been selected for this study (Figure 1). A more detailed description of
169 these samples is found in Elliott et al. (1997), who report the major-, trace-element
170 concentrations and Th, Sr, Pb and Nd isotopic compositions of the same samples. In addition,
171 several studies regarding the stable isotope ratios of those same samples are available in the
172 literature (Bouman et al., 2004; Eiler et al., 1997; Freymuth et al., 2015; Prytulak et al., 2013a,
173 2013b; Savage et al., 2010; Williams et al., 2018).

174
175 Ocean drilling program (ODP) sites 800, 801 and 802 were drilled during Leg 129
176 seaward of the Mariana arc. The drilling aim was to sample the altered Pacific crust and its
177 Jurassic-to-present sedimentary cover (Larson and Lancelot, 1992). The samples recovered

178 from Site 801 currently represent the primary reference site for subducted inputs to the
179 Mariana arc (Pigafetta basin and East Mariana basin located in Figure 1; see Plank (2013)
180 and references therein for details). The sedimentary column at Site 801 documents the plate's
181 voyage northwestward across the Pacific (Karpof, 1992), initially accumulating red clays (Unit
182 V) in the Jurassic, followed by radiolarites (Unit IV) when passing beneath the high
183 productivity belt at low latitudes. The biosiliceous accumulations of Units IV and II are
184 interrupted by intervals of volcanoclastic turbidite deposition (Unit III), due to underwater lava
185 flow outpourings and flank collapses of nearby seamounts in the mid-Cretaceous (Salimullah,
186 1992). The last 50-60 Ma of sediment deposition are condensed within the upper 50 meters of
187 the site 801 in Unit I, which is composed of pelagic red clay, recording periods when the site
188 entered the barren central gyre of the Pacific, far from terrigenous inputs and low in biologic
189 productivity. Thus, most of the sedimentary section is composed of biosiliceous cherts and
190 radiolarites and Cretaceous volcanoclastics, all selected to be studied here (8 samples from
191 Site 801 and 2 additional volcanoclastics from Site 802 to the south). A detailed description
192 and the stratigraphic section at Site 801 are given in Figure 2 and Table 1, together with the
193 location of our samples. The samples analyzed here are representative of the entire range in
194 Ce anomaly (Figure 2).

195
196 Basalts from the Mariana Trough (MTB) sometimes have trace elements and water
197 contents similar to those of Mid-Ocean Ridge Basalts (MORB). The majority of them however
198 is likely to be contaminated by fluids from the subducted Pacific slab. In this case samples are
199 enriched in fluid mobile elements (Rb, Ba, K and Pb), and therefore have intermediate
200 compositions between MORBs and arc lavas (Pearce et al., 2005). Our southern MTB
201 samples were recovered during the Cook 7 expedition (R/V Melville-2001) from an area along
202 the back-arc spreading axis that is ~4 km under sea level and where the distance between
203 the spreading center ridge and the magmatic arc front decreases from 106 to 33 km (Figure
204 1), providing the means to probe the relation between back-arc magmatism and the adjacent
205 volcanic arc front. Three southern MTB samples have been analyzed for both REE contents
206 and Ce-Nd isotopes.

207

208 Finally, three Pacific MORB samples (unaltered glasses) have been analyzed as
209 proxy for the background upper mantle isotopic composition. The Searise-1 DR05 sample
210 was dredged during the Searise-1 cruise in 1980 (2.28°N-102.78°W), the Cyana CY82
211 sample is a submersible-collected sample from the Cyana expedition in 1982 (12.72°N-
212 103.91°W) and the Clipperton DR01 sample (dredge) is from the Clipperton cruise in 1981
213 (12.75°N-103.93°W). Two additional Pacific MORB samples were previously analysed at the
214 Laboratoire Magmas et Volcans (LMV) and published in Bellot et al. (2015). All these samples
215 do not show any anomalous characteristics in terms of mantle heterogeneity (they all have
216 similar REE patterns and they do not show any DUPAL signature) nor do they indicate a deep
217 mantle signature based on their Hf and Nd isotope ratios (Chauvel and Blichert-Toft, 2001).

218

219

220 3. Analytical procedures

221

222 REE concentrations of all Mariana samples (arc basalts and Mariana Trough basalts), of
223 MORB sample Searise-1 DR05 and of 3 of the sediments (801B-12R, 802B-19 and 802B-
224 43R) were measured at LMV Clermont-Ferrand. All other REE data are from the literature
225 (see Table 1). In order to determine the REE concentrations, 100 mg of each sample were
226 digested in Savillex[®] beakers in a 3:1 mixture of 48% HF and 65% HNO₃ for 48 hours at
227 75°C. Before evaporation, 200 µl of HClO₄ acid were added to expel the fluorides. For
228 sedimentary samples, a preliminary degassing procedure using a 7M-HNO₃:2M-HCl mixture
229 was carried out in order to destroy the potentially carbonated and calcic components
230 (Carpentier, 2007). After the dissolution, samples were dissolved in 6M HCl and a 5% aliquot
231 was uptaken for the measurement of REE concentrations whereas the remaining 95% of the
232 sample was used for Ce and Nd isotope measurements. For REE measurements samples
233 were firstly dissolved in 7M HNO₃ to obtain a dilution factor of ~250, and measurements on
234 the Inductively Coupled Plasma Mass Spectrometer (ICP-MS) were performed with a final
235 dilution factor of 3500 in 0.45M HNO₃ – 0.05M HF. Two rock standards (Icelandic basalt BIR-
236 1 and Hawaii basalt BHVO-2) and one blank were dissolved using the same procedure.
237 Measurements were performed using the LMV Agilent 7500 quadrupole mass-spectrometer.

238 All calculations to transform peak signals into concentrations were performed offline. A blank,
239 bulk rock standards and a synthetic solution (CMS) containing ~ 60 trace elements at 1 ppb
240 were run every 4 Mariana samples throughout the entire sequence.

241
242 The Ce chemical separation protocol, described in detail in Bellot et al. (2015), requires
243 three steps: 1) isolation of the REE from the major elements which is carried out on AGW50-
244 X8 resin using 2.5M and 4M HCl acids; 2) the Ce and the Nd are separated on an AGW50-X8
245 resin using 0.27M 2MLA (α -hydroxyisobutyric) acid; and finally 3) the Ce fraction is purified
246 from residual Nd on Ln-Spec resin using 0.2 M HCl acid. The Nd fraction collected on the
247 second column is purified from Sm using a Ln-Spec resin and 0.25 M HCl (Pin and Santos
248 Zaldueguit, 1997). Cerium and Nd blanks were regularly measured by ICP-MS. The Nd
249 blanks were in the range of 22-39 pg whereas Ce blanks were between 44 and 339 pg. Those
250 values are negligible relative to the large quantity of Nd and Ce ($> 1\mu\text{g}$) processed for each
251 sample.

252
253 Cerium and Nd isotopes were measured using a Thermo Scientific Triton Thermal-
254 Ionization Mass Spectrometer (TIMS) at the LMV in Clermont-Ferrand. Instrumental mass
255 bias effects on Nd were corrected using an exponential law and $^{146}\text{Nd}/^{144}\text{Nd}=0.7219$
256 (Hamilton et al., 1983). Repeated measurements of the JNdi-1 Nd standard during the course
257 of this study gave an average $^{143}\text{Nd}/^{144}\text{Nd}$ ratio of 0.512107 ± 4 (2 standard deviation (2SD); n
258 = 14) in agreement, within error, with the value published in Tanaka et al. (2000). The Ce
259 isotope compositions were analyzed as oxide species using double Re filaments (Bellot et al.,
260 2015; Doucelance et al., 2014). The potential interferences of Ba, La, Pr and Nd were
261 monitored during the TIMS measurements. In oxide forms they are always negligible. The
262 purity of the Ce fraction after the chemistry was always checked by ICP-MS before isotope
263 analysis. The signal measured by ICPMS in our samples for La, Pr and Nd was similar to the
264 blank level showing that the Ce purification is faultless. Cerium isotope ratios were corrected
265 for the mass bias using an exponential law and $^{136}\text{Ce}/^{142}\text{Ce} = 0.01688$ (Makishima et al.,
266 1987). The $^{138}\text{Ce}/^{142}\text{Ce}$ analyses were carried out during 4 analytical sessions. The ^{140}Ce
267 tailing effect was quantified in each session because of its variability through time (Bellot et

1
2
3
4
5
6
7
8
9
10
11
12
13
14
15
16
17
18
19
20
21
22
23
24
25
26
27
28
29
30
31
32
33
34
35
36
37
38
39
40
41
42
43
44
45
46
47
48
49
50
51
52
53
54
55
56
57
58
59
60
61
62
63
64
65

268 al., 2015). Here we note a tailing correction on the $^{138}\text{Ce}/^{142}\text{Ce}$ ratio that varies from 0.5 to 1.2
269 ϵ -unit after mass bias correction. The Ce reference material solution AMES was measured at
270 least once a day for Ce isotopes (between 5 and 19 times for each session; Supplementary
271 file A). The drift of 49 ppm for the mean AMES $^{138}\text{Ce}/^{142}\text{Ce}$ ratio between the 4 sessions is
272 attributed to ageing of the Faraday cup. The AMES mean $^{138}\text{Ce}/^{142}\text{Ce}$ ratios have been
273 normalized to 0.0225746 ± 9 , a value obtained with the LMV TIMS for this standard during a
274 previous analytical session in which chondrites were measured to define the Chondritic
275 Uniform Reservoir (CHUR) reference value (Bellot et al., 2015). The epsilon value for this
276 standard solution is 4.13. The same AMES reference material analyzed by Willbold (2007)
277 and Willig and Stracke (2017) gave $^{138}\text{Ce}/^{142}\text{Ce}$ ratios of 0.0225749 ± 5 and 0.0225747 ± 5
278 respectively, in good agreement with our measurements. The external reproducibility (2SD)
279 calculated from the repeated AMES measurements within one session is in the range of 0.39
280 to 0.57ϵ -unit ($n=19$ to 5 ; Supplementary file A). The Ce reference material solution JMC-304
281 measured during session 1 gave a $^{138}\text{Ce}/^{142}\text{Ce}$ ratio of 0.0225704 ± 11 ($\epsilon\text{Ce}= 2.22\pm 0.51$ (2SD);
282 $n=3$, Supplementary file A). The Hawaii basalt standard BHVO-2 was measured during
283 session 2 and its $^{138}\text{Ce}/^{142}\text{Ce}$ is 0.0225643 ± 3 ($\epsilon\text{Ce}= -0.49\pm 0.13$).

286 4. Results

287 4.1. Cerium anomalies in Mariana arc

288
289 REE concentrations measured in Mariana lavas, as well as in Mariana Trough Basalts,
290 sediments and Pacific MORBs are presented in Table 1. REE concentrations in sediments
291 are from literature (Vervoort et al., 2011) except three sedimentary samples (801B-12R,
292 802A-19R and 802A-43R) that have been analyzed here (Table 1). USGS BHVO-2 (Hawaii
293 basalt) reference material was used to calibrate the signal considering the compilation given
294 in the GeoReM online database of Chauvel et al. (2011). Results obtained for the USGS BIR-
295 1 (Icelandic basalt) standard are in agreement with certified values, with a difference of less
296 than 5% in REE, and the external reproducibility (2SD) estimated from 4 measurements is
297 between 1% for Nd and 4% for Eu. In order to calculate the Ce anomaly, two methods of

1
2
3
4
5
6
7
8
9
10
11
12
13
14
15
16
17
18
19
20
21
22
23
24
25
26
27
28
29
30
31
32
33
34
35
36
37
38
39
40
41
42
43
44
45
46
47
48
49
50
51
52
53
54
55
56
57
58
59
60
61
62
63
64
65

298 calculation have been compared (Supplementary file B): 1) using the concentrations
299 calculated with the BHVO-2 standard as calibrator; 2) by calibrating the signal relative to the
300 CMS solution. They give consistent results with differences always smaller than 0.02 on the
301 cerium anomaly. Results obtained with the first calculation method are used in the discussion.
302 The Ce/Ce^* ($Ce_N / (La_N^{0.5} \times Pr_N^{0.5})$) values calculated for the two USGS rock standards BIR-1
303 and BHVO-2 using the second method of calibration are equal to 0.961 ± 0.006 (2SD, $n=4$)
304 and 1.005 ± 0.006 (2SD, $n=4$), respectively, which corresponds to a reproducibility better than
305 1%. Moreover, our BIR-1 results are in excellent agreement with the values of 0.957 ± 0.027
306 (2SD, $n=6$) published by Chauvel et al. (2011). A compilation of BIR-1 measurements is
307 reported in Pourmand et al. (2012) and the Ce anomaly in this rock standard is comprised
308 between 0.93 and 0.99 (average value of 0.96 ± 0.04 , 2SD, $n=11$). BIR-1 and BHVO-2 Ce
309 anomalies are also consistent with the Ce/Ce^* values calculated from certified concentrations:
310 0.97 and 1.01 for BIR-1 and BHVO-2, respectively. Our trace element data for Mariana arc
311 samples are in excellent agreement within 2% with values published by Elliott et al. (1997)
312 (Supplement file C). The Ce anomalies in Mariana arc lavas are all negative, ranging from
313 0.90 to 0.97. There is a 1% offset to higher Ce/Ce^* in the values determined here in
314 comparison to previous published values, perhaps due to Ca perchlorate interference on the
315 light REE (Longerich, 1993) or slight differences in the calibration values for BHVO-2.
316 Sediments show a larger range in Ce/Ce^* than lavas. They vary from 0.59 in sample 801A-8R
317 to 1.06 in sample 802A-19R.

4.2. Ce and Nd isotopes

320
321
322 The measured $^{138}Ce/^{142}Ce$ and $^{143}Nd/^{144}Nd$ ratios for Mariana arc samples, Mariana
323 Trough Basalts, Mariana trench sediments and the selected Pacific MORBs are presented in
324 Table 2. They are currently expressed in the epsilon notation (see Table 2 for values and
325 calculations). The Mariana arc samples have negative ϵ_{Ce} ranging from -0.84 (GUG-6) to -
326 0.45 (URA-7). The ϵ_{Nd} values of the same samples range from 6.01 (GUG-3) to 8.07 (GUG-

1
2
3 328 9). The MORB samples have ϵ_{Ce} from -1.65 to -0.77 and ϵ_{Nd} between 9.69 and 10.56, with
4
5 329 mean values of -1.08 and 9.99 for ϵ_{Ce} and ϵ_{Nd} , respectively. The isotope data we report here
6
7 330 is in good agreement with previous measurements of Ce isotopes in MORBs, whose mean
8
9 331 ϵ_{Ce} is -0.90 and mean ϵ_{Nd} is 9.73 (Bellot et al., 2015; Doucelance et al., 2014; Makishima and
10
11 332 Masuda, 1994). The three MTB samples yield heterogeneous Ce and Nd isotopic
12
13 333 compositions. Sample D68-2-1 has Ce and Nd isotopic compositions similar to that of MORB
14
15 334 end-member ($\epsilon_{\text{Ce}} = -1.13$; $\epsilon_{\text{Nd}} = 9.79$). The two other back-arc basalts have compositions
16
17 335 similar to those of the basaltic Mariana arc lavas. Isotope results are consistent with the
18
19 336 conclusions of Pearce (2005) based on trace-element measurements since D68-2-1 was the
20
21 337 only analysed sample collected in a segment of the south Mariana Trough that was identified
22
23 338 as a MORB-like domain, *i.e.* without contamination by slab fluids.

24
25 339 For the Mariana trench sediments, the isotopic ratios of volcanoclastic turbidites are quite
26
27 340 homogeneous and range from -0.13 to 0.29 and from 0.97 to 5.17 for ϵ_{Ce} and ϵ_{Nd} ,
28
29 341 respectively. The Nd isotope compositions of the same samples were already measured for
30
31 342 the 2 volcanoclastic samples 801B-5R and the 801B-8R (Vervoort et al., 2011). Our results
32
33 343 are in agreement with these earlier results to within 30 ppm, a difference that can be
34
35 344 attributed to powder heterogeneity. In comparison to volcanoclastics, the biosiliceous
36
37 345 sediments have more variable Ce and Nd isotope ratios with ϵ_{Ce} ranging from 0.30 to 1.15
38
39 346 and ϵ_{Nd} from -8.64 to -0.79. The large isotopic variations in the biosiliceous sediments reflect
40
41 347 a broad lithological diversity.
42
43
44
45
46
47
48
49

50 349 5. Discussion

51
52 350
53
54 351 The lava samples analysed in this study have ϵ_{Nd} and ϵ_{Ce} that differ from those of MORB
55
56 352 samples. In order to explain such variations, we develop mixing models between the local,
57
58 353 depleted mantle and two distinct components derived from recycled sediments. In a second
59
60
61
62
63
64
65

1
2
3
4
5
6
7
8
9
10
11
12
13
14
15
16
17
18
19
20
21
22
23
24
25
26
27
28
29
30
31
32
33
34
35
36
37
38
39
40
41
42
43
44
45
46
47
48
49
50
51
52
53
54
55
56
57
58
59
60
61
62
63
64
65

354 step, we detail other potential factors that could influence the rare earth element contents of
355 the lavas and potentially generate Ce anomalies..

356

357 **5.1. Ce-Nd isotope constraints on the origin of Ce anomalies in Mariana lavas**

358

359 Mariana arc samples show a co-variation in ϵ_{Nd} vs. Ce/Ce* diagram (Figure 3A). The co-
360 variation is less well defined in the ϵ_{Ce} vs. Ce/Ce* plot (Figure 3B) because the total variation
361 in Ce isotope composition is small. The Sm-Nd systematics confirms that the Ce anomalies
362 are mostly source-related, in agreement with the conclusions of Elliott et al. (1997).
363 Biosiliceous and volcanoclastic trench sediments possess distinct $^{138}Ce/^{142}Ce$ and $^{143}Nd/^{144}Nd$
364 isotope ratios (Table 2). Thus binary mixing models between the depleted mantle (mantle
365 wedge) and the two types of sedimentary components (biosiliceous vs volcanoclastic) may
366 help to better constrain the nature and the proportions of sediments involved in Mariana arc
367 volcanism. Is a specific material responsible for the presence of the Ce anomalies and for the
368 Ce and Nd isotopic compositions in the Mariana arc lavas? For model purpose, no age
369 correction was applied to the sediments. The drilled samples are considered as
370 representative of the subducted sediments involved in the source of the current volcanism at
371 the Mariana arc. The Mariana arc- trench system is of intra-oceanic type and the pelagic
372 background sedimentation is slow. Moreover the fore-arc topography and geophysical
373 imaging reveal that all of the trench sediment is subducted. With these arguments we can
374 assume that the same type of sedimentary material was indeed subducting in the past.

375

376

377 An important input parameter is the light REE (LREE) concentrations of the DMM end-
378 member. Several estimates have been published however we note significant differences in
379 the proposed concentrations. For example the Ce concentration is 1.4 times higher in the
380 DMM composition of Salters and Stracke (2004) when compared with that of Workman and
381 Hart (2005) and these two DMM-models have Ce/Ce* of 1.05 and 0.91, respectively. The
382 Mariana Trough Basalt D68-2-1 collected in a MORB-like domain segment (Pearce et al.,

1
2
3
4
5
6
7
8
9
10
11
12
13
14
15
16
17
18
19
20
21
22
23
24
25
26
27
28
29
30
31
32
33
34
35
36
37
38
39
40
41
42
43
44
45
46
47
48
49
50
51
52
53
54
55
56
57
58
59
60
61
62
63
64
65

383 2005) yields a REE pattern similar to N-MORB (Figure 4) and has no cerium anomaly
384 ($Ce/Ce^*=1.00$). Comparing the different elemental ratios (La/Ce, Ce/Nd, Nd/Pr) in DMM end-
385 members and the sample D68-2-1, we note that the La/Ce ratio shows the greatest difference
386 (9% instead of 2% for Ce/Nd and Nd/Pr). When Ce/Ce^* is calculated without considering La
387 ($Ce^*=(Pr \times (Pr/Nd))$), Lawrence et al., 2006) the cerium anomaly in Salter and Stracke (2003)
388 DMM disappears ($Ce/Ce^*=0.99$). These observations suggest that the concentration in La in
389 this end-member is too low. The La content in Salters and Stracke (2004) DMM is increased
390 from 0.234 ppm to 0.265 ppm in order to reproduce the La/Ce ratio measured in the basalt
391 D68-2-1 (equal to 0.331). With such a La content the Ce anomaly is removed and the value
392 fits perfectly within the MORB field in the La/Ce vs. La plot presented in Salters and Stracke
393 (2004; see their Figure 2). There is no negative Ce anomaly in rocks sampling the depleted
394 mantle in the literature, with rare exceptions that are commonly attributed to seafloor
395 weathering and low temperature processes (e.g. Makishima and Masuda, 1994).

396
397 Another important input parameter is the REE content of the sediment-derived component
398 involved in the source of Mariana basalts. We used the estimated P-T conditions of Syracuse
399 et al. (2010) to evaluate the behavior of Ce and Nd under the Mariana volcanic arc. For
400 hydrated metapelites, these conditions correspond to a transition from aqueous fluids to
401 hydrous melts (Hermann and Spandler, 2008). The hydrous melts are the result of partial
402 melting of sediment in the presence of water. The partial melting of sediments leads to more
403 efficient recycling of LREE when compared to the simple sediment dewatering, although
404 experimental data compiled in Plank et al. (2009) show the strong effect of temperature on
405 the solubility of the REE. Most of the experiments reveal that Ce is not fractionated in
406 comparison to its neighboring elements (Martindale et al., 2013; Skora and Blundy, 2012). To
407 our knowledge only the recent study of Tsay et al. (2017), which conducted experiments on
408 the dehydration of an allanite-bearing eclogite at 2.5 GPa and 600-800°C, obtained aqueous
409 fluids characterized by positive Ce anomalies. However the Ce anomalies on the fluid/(bulk)
410 solid partition coefficients are not resolved when the analytical uncertainties are considered.
411 Here results on high-P/high-T experiments on sedimentary materials are used to constrain the
412 behavior of Ce and Nd, and in particular their partition coefficients in each of the two types of

1
2
3
4
5
6
7
8
9
10
11
12
13
14
15
16
17
18
19
20
21
22
23
24
25
26
27
28
29
30
31
32
33
34
35
36
37
38
39
40
41
42
43
44
45
46
47
48
49
50
51
52
53
54
55
56
57
58
59
60
61
62
63
64
65

413 sedimentary materials: biosiliceous sediments from Johnson and Plank (1999) and in
414 volcanoclastics ones from Martindale et al. (2013).

415

416

417 **5.1.1. Biosiliceous sediments**

418

419 The high-P/high-T experiments of Johnson and Plank (1999) used natural pelagic red clay
420 from the eastern Tonga Trench (DSDP site 595). This type of sediment is common amongst
421 the sediments from the Pacific ocean (Plank and Langmuir, 1998). It is also comparable to the
422 red clays of Unit I and to the non-biogenic fraction of Units II, IV and V at Site 801, east of the
423 Mariana arc front (Figure 2). In the calculations, the concentrations measured in the
424 biosiliceous samples (Vervoort et al., 2011; this study) are multiplied by the enrichment factor
425 reported in Table 3. Sediments produced partial melts in these conditions, and not aqueous
426 fluids. They are depleted in REE in comparison to the initial sediment.

427

428 Figure 5A shows the binary mixing curves in $\epsilon_{\text{Ce}}-\epsilon_{\text{Nd}}$ space between D68-2-1 and
429 components derived from the biosiliceous sediments. The two samples 801A-17R and 801B-
430 33R (a porcellanite and a radiolarite, respectively) cover the entire ϵ_{Ce} biosiliceous sediment
431 range; thus their isotopic compositions are used to constrain those of the two enriched end-
432 members in the calculated mixing curves. Concentrations used in the model correspond to
433 the average concentration of biosiliceous sediments. Both mixing curves pass through the
434 Mariana arc samples within the error bars on the measurements. The incorporation of 2.5% to
435 8% of melts extracted from biosiliceous sediments reproduces the $^{138}\text{Ce}/^{142}\text{Ce}$ and
436 $^{143}\text{Nd}/^{144}\text{Nd}$ ratios of the Mariana arc samples. This model must also explain the Ce/Ce*
437 values measured in the same samples. The calculated Ce/Ce* values are presented in Figure
438 5B relative to the sedimentary proportions. For the proportion of sedimentary component
439 determined using Ce-Nd isotopes (2.5% to 8%), the calculated Ce/Ce* values in the Mariana
440 arc samples range from 0.91 to 0.84. These values are significantly lower than Ce/Ce* values
441 (up to 0.90) measured in lavas (Figure. 5B). Results are similar when the mean Ce-Nd

442 isotope composition is considered for the sedimentary end-member (see supplementary
443 material D).

444

445

446 **5.1.2. Volcaniclastic sediments**

447

448 Our calculations are based on the results obtained experimentally by Martindale et al.
449 (2013) on the volcaniclastic sediment 801B-8R3. The Ce, Pr and Nd concentrations of the
450 fluids were calculated considering the partition coefficients in the 850°C-3GPa experiment
451 (see Table 5 of Martindale et al. (2013) and our Table 3) and the concentration in this
452 volcaniclastic sample published in Vervoort et al. (2011). Because enrichment factors are
453 higher than 1, melts are enriched in REE relative to the initial material. The two mixing lines
454 shown in Figure 6A join the local depleted mantle (with an isotopic composition identical to
455 that of D68-2-1) and two distinct enriched end-members which Ce and Nd isotopic ratios
456 correspond to those of the two volcaniclastic sediments with the most extreme Ce isotope
457 compositions (801B-8R3 and 801B-7R, respectively). Concentrations correspond to the mean
458 value of all volcaniclastic samples. Both curves pass through the lava arc samples within the
459 error bars on the Ce isotope measurements. To explain the $^{138}\text{Ce}/^{142}\text{Ce}$ and $^{143}\text{Nd}/^{144}\text{Nd}$ ratios
460 of the Mariana arc lavas, 0.75% to 2.75% melt from volcaniclastic sediments is necessary.
461 Such a contribution would produce arc magmas that are characterized by a Ce/Ce* of 0.97 to
462 0.95 (Figure 6B). These values are in agreement with the majority of cerium anomalies
463 measured in our samples. One of the four studied volcaniclastic samples (802-43R from site
464 802) has a Ce/Ce* of 0.88, which is significantly lower than those measured in the other three
465 samples (from 0.91 to 1.06). However, this very low Ce/Ce* value is unique among the 13
466 measured volcaniclastic samples found in the literature, with a range of Ce/Ce* comprised
467 between 0.88 to 1.06 ($N = 13$; Karpof, 1992; Vervoort et al., 2011; this study). The
468 participation in small proportion of the component derived from volcaniclastic sediments
469 satisfies both Ce-Nd isotope compositions and the Ce anomalies of the Mariana arc. Results
470 are similar when the mean Ce-Nd isotope composition of volcanoclastics is considered for the
471 sedimentary end-member (see supplementary material E).

472

473

474 5.1.3. Comparison with previous estimates

475

476 Fluids/melts from the most common sediments (biosiliceous and volcanoclastic) drilled off
477 the Mariana Trench at ODP sites 801 and 802 must have directly participated in the arc
478 magma genesis as evidenced by some key trace element abundances characteristic only to
479 sediments (Elliott et al., 1997; Ishikawa and Tera, 1999; Plank and Langmuir, 1998b). Our
480 calculations show that the melting of subducted volcanoclastics contributed smaller Ce
481 anomalies than the biosiliceous ones and the sedimentary proportions calculated from Ce-Nd
482 isotope data are also smaller for volcanoclastics than for biosiliceous sediments (0.75-2.75%
483 against 2.5 to 8%). The participation of sediments in the source of the Mariana arc lavas has
484 been studied using a large range of geochemical tools, including trace elements and isotope
485 systematics and all results converge towards a sedimentary proportion that does not exceed
486 4% (^{238}U - ^{230}Th , ^{147}Sm - ^{143}Nd , ^{176}Lu - ^{177}Hf , U-Th-Pb) (Avanzinelli et al., 2012; Elliott et al., 1997;
487 Hole et al., 1984; Tollstrup and Gill, 2005; Vroon et al., 1995; White and Dupré, 1986;
488 Woodhead, 1989). Our Ce-Nd results give sedimentary proportions that agree generally well
489 with these previous estimates if the sedimentary component is derived from volcanoclastics
490 whereas the sedimentary proportion can be up to 8% for biosiliceous sediments and then far
491 above the previous estimates. Moreover with biosiliceous sediments we cannot reproduce
492 both the Ce-Nd-isotope compositions and the cerium anomalies of the lavas. It would be
493 interesting to calculate a bulk sediment Ce isotope composition for the ODP site 801 but this
494 is currently impossible because 1) the number of samples analyzed in this study is too small;
495 2) no samples from unit 1 of this site were analyzed, and 3) published measurements of
496 $^{138}\text{Ce}/^{142}\text{Ce}$ ratios in sediments are very scarce and exist only for Lesser Antilles forearc
497 sediments (Bellot et al., 2015). Unfortunately we did not identify any good chemical proxy for
498 the Ce isotope composition of the Mariana Trench sedimentary column.

499

500 We also show the importance of considering the compositions of the sediments on the
501 seafloor near to the deep-sea trench. The very low sedimentary melt proportions of 0.4% for

1
2
3
4
5
6
7
8
9
10
11
12
13
14
15
16
17
18
19
20
21
22
23
24
25
26
27
28
29
30
31
32
33
34
35
36
37
38
39
40
41
42
43
44
45
46
47
48
49
50
51
52
53
54
55
56
57
58
59
60
61
62
63
64
65

502 Mariana arc samples calculated in Hole et al. (1984) to explain their Ce anomalies is a direct
503 reflection of the importance of the choice of mixing end-members. They use the PAWMS
504 (Pacific Authigenic Weighted Mean Sediment) representing the mean concentrations for
505 DSDP Leg 34, Hole 314, located on Nazca plate in the east Pacific Ocean. This material has
506 a very large Ce anomaly (Ce/Ce^* of 0.2) compared to sediments located seaward of the
507 Mariana arc front. This observation illustrates the caveats of using average global
508 compositions to quantify the sources contributing to subduction zone-related magmas, in
509 agreement with Woodhead et al. (2012).

512 **5.2. Ce anomalies in worldwide magmatic arcs: can other processes generate cerium** 513 **anomalies?**

514
515 The compilation of Ce/Ce^* measured in arcs from the geochemical database GEOROC
516 reveals that several subduction zones are characterized by volcanic rocks with negative Ce
517 anomalies, i.e. Central America, the Cascades, Izu-Bonin and Mariana arcs (Figure 7).
518 However, sediments drilled within the trench do not have systematically cerium anomalies
519 (e.g. Cascades). Working on databases has the advantage of bringing out trends but here no
520 data filtering has been applied. We are aware that cerium anomalies are small and only
521 rigorous analytical works can reliably quantify these small variations. Also negative Ce
522 anomalies can result from secondary processes when subaerial basalts are exposed to
523 alteration in tropical environments. This has been found for basalts from French Polynesian
524 islands (Cotten et al., 1995). In this case, the negative Ce anomalies in the basalts result from
525 the precipitation of Y-REE rich phosphates concentrating all REE except Ce. Such
526 precipitates remain rare and are not observed in our Mariana samples. The Mariana arc
527 samples have quite similar REE abundances (Table 1) and their chondrite-normalized values
528 fall between 10 and 100 (Log space) in comparison with 1000 as is the case in arc lavas with
529 Y-REE rich phosphate precipitation. Also, the La/Nb, Nd/Zr or Sm/Hf ratios are all similar and
530 not significantly elevated as would be expected with Y-REE rich phosphates (Cotten et al.,
531 1995). Lastly, the Mariana arc samples are all historic or young enough (<350ka) to have

1
2
3
4
5
6
7
8
9
10
11
12
13
14
15
16
17
18
19
20
21
22
23
24
25
26
27
28
29
30
31
32
33
34
35
36
37
38
39
40
41
42
43
44
45
46
47
48
49
50
51
52
53
54
55
56
57
58
59
60
61
62
63
64
65

532 significant U-Th disequilibria, so they should not have experienced such extensive weathering
533 (Elliott et al., 1997).

534 The formation of cerium anomaly by magmatic processes such as partial melting and/or
535 fractional crystallization has never been thoroughly examined. We test below the potential
536 influence of magmatism on the Ce/Ce* values in the context of the formation of arc lavas.
537 Since coupled Ce/Ce* and ϵ Ce data are now available in lavas of two different island arcs
538 (Antilles and Mariana), our calculations have been applied to these particular cases.

539

540 **5.2.1. Batch melting**

541

542 The models are based on the proposed slab geometry beneath volcanic arcs by Syracuse
543 and Abers (2006). Beneath the Mariana volcanic arc front the slab depths vary from 172 to
544 156 km (north-south). The pressure-temperature conditions at these depths are estimated to
545 be 5-5.5 GPa and 780-820°C (model D80 in Syracuse et al., 2010). In the south part of the
546 Lesser Antilles the slab depth is about 140 km corresponding to pressure-temperature
547 conditions of 4-5 GPa and 780°C (model D80 in Syracuse et al., 2010). Under these
548 conditions, melting occurs in the garnet stability field. Thus we have considered a garnet
549 peridotite with the following modal abundance: 55% olivine, 11% clinopyroxene, 25%
550 orthopyroxene and 9% garnet (Rollinson, 1993). Because Mariana arc samples and most of
551 those analysed for Lesser Antilles do not have a garnet signature (fractionation between
552 heavy REE), we can also assume that melting continues into the spinel stability field, or that
553 garnet is consumed. A second composition has been then modelled with the reduction of the
554 garnet content from 9% to 6% and by adding 3% spinel. Mantle wedge metasomatism also
555 needs to be integrated into the model. As a first approximation, we consider that the depleted
556 sub-arc mantle was contaminated by 2% of melt extracted from volcanoclastic sediments
557 fluids (case of Mariana) or 5% fluids coming from the partial melting of the GLOSS-II reservoir
558 (case of Martinique Island following the proportion estimated in Bellot et al., 2015). The fluid
559 composition is calculated by applying the bulk solid/fluid partition coefficients measured from
560 the experiments carried out by Martindale et al. (2013) for Mariana and by Johnson and Plank
561 (1999) for Lesser Antilles. We then assume cryptic metasomatism, in which the bulk

1
2
3
4
5
6
7
8
9
10
11
12
13
14
15
16
17
18
19
20
21
22
23
24
25
26
27
28
29
30
31
32
33
34
35
36
37
38
39
40
41
42
43
44
45
46
47
48
49
50
51
52
53
54
55
56
57
58
59
60
61
62
63
64
65

562 chemistry of the mantle wedge is modified by metasomatism but without bulk mineralogical
563 changes. It is likely that the fluid/melt circulation would have resulted in mineralogical
564 reactions and the occurrence of hydrous minerals. These phases would have been consumed
565 immediately by melting and would probably not play any significant role subsequently. In our
566 model the LREE concentrations of the mantle source are those proposed by Salters and
567 Stracke (2004) for the depleted mantle. The bulk partition coefficients (D) of the garnet-spinel
568 peridotite are determined from K_D values proposed by McKenzie and O’Nions (1991) for each
569 basalt/mineral phase proportion. We choose McKenzie and O’Nions K_D values because their
570 study is the only study given all K_D necessary for our model. The change of Ce/Ce^* ,
571 expressed in $\Delta Ce/Ce^*$ (normalized to the initial composition equal to 100% of partial melt) is
572 plotted against the degree of partial melting (%). Results presented in Figure 8A show that
573 variation is always very small and lower than 0.021. The maximum Ce/Ce^* variation is
574 obtained for 2.5% melting. The spinel peridotite composition results in smaller variations than
575 the garnet composition. The change in the sediment proportion (2 to 5%) and its composition
576 (volcaniclastic vs GLOSS) does not modify the calculated curves. Partial melting generates
577 small variation of the cerium anomaly and its potential effect has not been considered in the
578 models presented in figures 5B and 6B. The cerium anomaly changes of 0.01 when
579 considering the typical melting degree for arc lavas, i.e. ~10%. Thus the melting process
580 increases the amplitude of the cerium anomaly and can explain the most extreme Ce/Ce^*
581 values of (0.90 to 0.92) measured in a few samples.

584 **5.2.2. Fractional crystallization**

585
586 Results of the fractional crystallization (FC) calculations are presented in figure 8B. The
587 initial magma corresponds to 10% of partial melting of the previously metasomatized depleted
588 mantle (see section 5.2.1 and figure 8A). The crystallizing mineral assemblage used here
589 results from 1) the modelling of Dixon and Batiza (1979) for Mariana (see Table 5 of their
590 paper); and 2) the propositions made in Labanieh et al. (2012) for andesites from Martinique
591 lavas. The bulk LREE solid/melt partition coefficients between the minerals (olivine, cpx, opx,

1
2
3
4
5
6
7
8
9
10
11
12
13
14
15
16
17
18
19
20
21
22
23
24
25
26
27
28
29
30
31
32
33
34
35
36
37
38
39
40
41
42
43
44
45
46
47
48
49
50
51
52
53
54
55
56
57
58
59
60
61
62
63
64
65

592 plagioclase, amphibole, garnet and/or magnetite) and the basaltic melt are calculated from
593 the partition coefficients $D^{\text{basalt/mineral}}$ of McKenzie and O'Nions (1991) except $D^{\text{basalt/magnetite}}$ for
594 LREE (Luhr and Carmichael, 1980). Because Pr was not measured in this last study, the
595 partition coefficient for this element has been calculated by linear interpolation between La
596 and Nd that are two elements existing only in 3+ valence state using the following equation:
597 $(1/3) \cdot K_D \text{La} + (2/3) \cdot K_D \text{Nd}$. This calculation shows that FC does not control the cerium anomaly
598 neither for the Mariana arc nor for Martinique samples with variation lower than 0.005 (Figure
599 8B). The difference in the lava mineralogy for the two arc systems explains the variations
600 observed in the figure 8B.. Several arguments show that FC does not control the trace
601 element composition neither for the Mariana arc nor for Martinique samples. Firstly, most of
602 our rocks plot on a positive straight line on diagrams using the ratios of two incompatible
603 elements such as Th/REE as a function of the concentration of the most incompatible element
604 (Th), suggesting that variations in trace elements are mostly controlled by batch melting
605 rather than FC (Figure 9). In addition, the Ce/Ce* and MgO contents of the arc samples do
606 not co-vary. In these two locations, sample that seem to be more affected by FC do not have
607 the lowest Ce/Ce* value. The influence of FC on the Ce anomalies is thus limited, especially
608 for Mariana lavas. Turning to Martinique lavas, Labanieh et al. (2012) have examined in great
609 detail the effect of the FC process on REE. They showed that amphibole and garnet are able
610 to fractionate REE ratios (e.g. La/Sm) in some particular volcanic complexes of Martinique
611 (Conil, Carbet, Pelée and Gros Ilet). Our calculations, however, show that FC does not
612 significantly fractionate Ce relative to its neighboring elements and does not generate Ce
613 anomaly in the lavas. Indeed these samples do not differ from the others in the figure 9B.

616 **5.2.3. The role of residual accessory mineral phases**

617
618 The role of residual accessory mineral phases present in subducted sediments has been
619 previously highlighted, in particular to explain the correlation observed between $^{176}\text{Hf}/^{177}\text{Hf}$
620 ratios and Hf concentrations in the Izu-Bonin-Mariana arc system (Tollstrup and Gill, 2005).
621 Thus, less than 2% of fluids coming from 25% of partial melting of subducted sediments are

1
2
3
4
5
6
7
8
9
10
11
12
13
14
15
16
17
18
19
20
21
22
23
24
25
26
27
28
29
30
31
32
33
34
35
36
37
38
39
40
41
42
43
44
45
46
47
48
49
50
51
52
53
54
55
56
57
58
59
60
61
62
63
64
65

622 needed, when associated with 0.0025% of residual zircon, to result in the six-fold increase of
623 the Nd/Hf ratio that is expected to explain the Hf anomalies measured in the Mariana arc
624 lavas (Tollstrup and Gill, 2005). Combined ^{238}U – ^{230}Th and ^{235}U – ^{231}Pa measurements on
625 Mariana lavas show that the main control on U-series in these samples is exerted by
626 accessory phases (allanite, monazite and zircon) present during the recycling of the
627 subducted material (Avanzinelli et al., 2012). Cerium is incompatible with respect to zircon
628 formed in hydrous veins at eclogitic facies conditions (Rubatto and Hermann, 2003). Zircon
629 retains Ce more efficiently than other REE, but its concentrations remain very low in
630 comparison to those observed in magmatic zircons (~2 ppm in zircon veins formed by
631 fluids/melts in subduction zones; Rubatto and Hermann, 2003). If zircon is present during
632 partial melting of the sediments, it might fractionate the HFSE more efficiently when
633 compared to the LREE. The same is true for rutile, whose Ce partition coefficient ($D^{\text{mineral/melt}}$)
634 is <0.001 (Klemme et al., 2005). The presence of residual accessory mineral phases in sub-
635 arc conditions can explain the HFSE signatures (Avanzinelli et al., 2012; Martindale et al.,
636 2013), but their influence seems to be limited for the LREE and does not explain any cerium
637 fractionation relative to its neighboring elements. Conversely, the dehydration of an allanite-
638 bearing eclogite seems to produce aqueous fluids characterized by positive cerium anomalies
639 (Tsay et al., 2017), but these anomalies are poorly constrained relative to the analytical
640 precision. Cerium anomaly ($\text{Ce}/\text{Ce}^* > 1$) increases with the temperature of the experiments.
641 This effect cannot be related to a redox effect because experiments made at higher
642 temperature are more reducing, as attested by the amplitude of the Eu anomaly, meaning that
643 the cerium should be present in the valence 3^+ i.e., like the other REE (Tsay et al., 2017).
644 Active serpentinite mud volcanism in the shallow fore-arc region of the Mariana convergent
645 margin presents a unique opportunity to characterize the slab-derived fluids. Here it has been
646 shown that relative to the depleted mantle wedge, the fluid mobile elements which are
647 characteristic of the subducted slabs (B, Cs, I, As, Sb; Snyder et al., 2004; Savov et al., 2005,
648 2007) are often orders of magnitude more enriched in the serpentinite muds and fluids
649 sampled from carbonate and brucite chimneys at the summits of these mud volcanoes. At the
650 low temperature (<350°C) of the fore-arc regions, the LREE remain immobile as no significant
651 decoupling between Ce, La and Pr has been identified (Savov et al., 2007, 2005).

652

653 **5.3.1. Effect of mantle redox conditions on Ce valence state**

654

655 The effect of the oxygen fugacity on the cerium valence state is well known in sub-surface
656 conditions but experiments in mantle conditions are very scarce. The presence of Ce⁴⁺ in
657 magmatic rocks has been first highlighted with the presence of positive cerium anomaly in
658 zircons. In this mineral the CI-normalized REE pattern is often characterized by the coupled
659 presence of positive cerium and negative europium anomalies. Cerium and Eu, unlike the
660 other REE, do not exclusively form trivalent ions, existing also as Ce⁴⁺ and Eu²⁺. The
661 partitioning between zircon and melt for these elements changes with the variations of the
662 oxygen fugacity (Burnham and Berry, 2012). The only other study presenting REE partition
663 coefficients for different reducing conditions is for plagioclase in basaltic melt (Aigner-Torres
664 et al., 2007). The melt in the later study lacks significant cerium anomaly despite the large
665 range of the oxygen fugacity investigated in the experiments ($fO_2 = IW, QFM, air$). However,
666 we note that the plagioclase/melt partition coefficient for cerium does not plot exactly on the
667 3+ curve in the lattice strain model of Aigner-Torres et al. (2007) but slightly below (see their
668 figure 5). The analytical precision of in-situ REE measurements representing a wide range of
669 relevant experimental conditions does not allow the detection of the Ce anomalies.

670

671 The oxidation state of Ce in silicate melt can be quantified using XANES technique
672 (Burnham and Berry, 2014; Smythe and Brenan, 2015). Ce⁴⁺/ΣCe in natural melts is
673 exceedingly small and seems to be recorded only in the mineral zircon that has a great
674 potential as an oxy-barometer (Smythe and Brenan, 2016; Trail et al., 2011). Smythe and
675 Brenan (2015) have determined a small fraction of Ce⁴⁺ under terrestrial magmatic conditions
676 in a large range of fO_2 for rhyolite to basalt compositions (FMQ varying from -4 to +8.4).
677 Using an oxygen fugacity of 2 log units above FMQ as value for magmas in subduction zones
678 (Kelley and Cottrell, 2009; Parkinson and Arculus, 1999), we estimate the Ce⁴⁺/Ce³⁺ ratio in a
679 basaltic arc melt of about 0.0012. In addition, in presence of Fe in natural silicate melts, the
680 enthalpy energy of oxidizing Fe (Fe²⁺ → Fe³⁺) is lower than the one for Ce (Burnham and
681 Berry, 2014; Schreiber et al., 1980) and the polymerization of the melt increases the redox

1
2
3
4
5
6
7
8
9
10
11
12
13
14
15
16
17
18
19
20
21
22
23
24
25
26
27
28
29
30
31
32
33
34
35
36
37
38
39
40
41
42
43
44
45
46
47
48
49
50
51
52
53
54
55
56
57
58
59
60
61
62
63
64
65

682 state of Ce contrarily to the addition of H₂O (Smythe and Brenan, 2015). In conclusion even if
683 basaltic melts near subduction zones are more oxidized than magmas from divergent plate
684 boundaries (Kelley and Cottrell, 2009), the redox conditions cannot generate Ce anomaly in
685 arc lavas.

686
687 The measurement of non-traditional stable isotopes has been developed with the aim of
688 better characterizing the mantle redox conditions. Cations such as Cr, Fe, Ti, and V exhibit a
689 range of valence states that depend on the stability of mineral phases and the partitioning
690 behavior between mineral and melt (Papike et al., 2005). Mariana arc samples have been the
691 subjects of several stable isotope studies, including Ti (Prytulak et al., 2013b), V (Prytulak et
692 al., 2017), Mo (Freymuth et al., 2015) and Fe (Williams et al., 2018). Although some of these
693 analyses were conducted on the Mariana samples studied here, no clear correlation is
694 observed between these isotopes and the Ce isotope ratios. A slight co-variation is observed
695 between Mo and Ce isotopes (n=5). Measured variations in Mo and Ce are too small relative
696 to the analytical errors to be clearly resolved (supplementary file F). Voegelin et al. (2014)
697 showed the absence of fractionation of Mo isotopes ($\delta^{98/95}\text{Mo}$) during fractional crystallization
698 in the specific case of Mariana arc magmas since all these samples present a narrow range in
699 MgO concentrations. Molybdenum isotope range in Mariana arc lavas is explained by the
700 participation of fluids from the lower subducted basaltic crust, where Mo isotopes would
701 fractionate during dehydration, and/or by the presence of residual rutile from the sediment
702 melts (Freymuth et al., 2015; Skora et al., 2017). However experimental studies realized so
703 far do not report any Ce fractionation in the presence of residual rutile.

704 705 706 **5.3.2 Implications of Ce-Nd isotopes in arc magma environments**

707
708 The first coupled Ce-Nd isotope measurements on island volcanic rocks were reported for
709 samples characterized by large negative cerium anomalies up to 0.73: 16 samples from two
710 Solomon Islands (Shortland and New Georgia) and 3 samples from Bonin Islands (Shimizu et
711 al., 1992). The compilation of all data available on samples collected in arc settings (lavas,

1
2
3
4
5
6
7
8
9
10
11
12
13
14
15
16
17
18
19
20
21
22
23
24
25
26
27
28
29
30
31
32
33
34
35
36
37
38
39
40
41
42
43
44
45
46
47
48
49
50
51
52
53
54
55
56
57
58
59
60
61
62
63
64
65

712 sediments) and mid-ocean ridge samples is presented in figure 10. We note that lavas from
713 Bonin and Solomon Islands have more radiogenic ϵ_{Ce} values than those from Mariana and
714 Martinique with comparable ϵ_{Nd} . Since no sediment collected near Bonin and Solomon
715 Islands has been analyzed, mixing curves cannot be calculated between depleted mantle and
716 enriched source as done for Mariana and Lesser Antilles. Only one enriched end-member
717 composed by sediments having very radiogenic $^{138}\text{Ce}/^{142}\text{Ce}$ ratios would explain the
718 measured isotope ratios in Bonin and Solomon arc samples. Radiogenic $^{138}\text{Ce}/^{142}\text{Ce}$ ratios
719 are acquired over time in reservoirs characterized by high La/Ce ratios and then usually
720 having very low Ce contents and much lower Ce/Nd ratios than that of the depleted mantle.
721 With these end-members, mixing calculations produce convex curves in the ϵ_{Ce} vs. ϵ_{Nd}
722 diagram that do not pass through the samples located in the upper-right quadrant. Mean
723 sedimentary piles calculated for Izu-Bonin (ODP Leg 185 Site 1149) and Vanuatu (DSDP Leg
724 30 Site 286) are both characterized by negative cerium anomalies (0.69 and 0.90,
725 respectively) close to that of the sedimentary column sampled at the Mariana trench (0.73).
726 The ϵ_{Nd} measured in DSDP Leg 30 Site 286 sediments are very high compared to those
727 measured in Mariana (+2 to +9 in Vervoort et al., 2011 and -2 to 10 in Peate et al., 1997). The
728 participation of a large quantity of sediments in the magma source is also excluded from
729 results on Hf, Nd, Sr and Pb isotopes measured in samples from Solomon Islands (Schuth et
730 al., 2009). In conclusion using the geochemical database of oceanic sediments collected in
731 this part of the Pacific Ocean, the cerium isotopic composition of Bonin and Solomon arc
732 samples remains enigmatic. Additionally, we have highlighted the need to use the “local”
733 mantle as depleted end-member in our Ce-Nd isotope mixing models for Mariana samples
734 (Mariana Through basalt instead of the mean MORB). The ϵ_{Ce} variability in MORB is up to
735 1.2, which is significant regarding the analytical precision of 0.4. To model Solomon samples,
736 it may be necessary to consider the presence of the Ontong Java plateau and of the Indian
737 mantle wedge trapped under Solomon Islands too. The local tectonic settings result in an
738 anomalously high mantle temperature and probably lead to the production of adakitic melts
739 (Schutl et al., 2009).

1
2
3
4
5
6
7
8
9
10
11
12
13
14
15
16
17
18
19
20
21
22
23
24
25
26
27
28
29
30
31
32
33
34
35
36
37
38
39
40
41
42
43
44
45
46
47
48
49
50
51
52
53
54
55
56
57
58
59
60
61
62
63
64
65

741 Martinique island lavas are of particular interest to understand magma generation in the
742 case of sediment incorporation into the mantle wedge because they all fit on hyperbolas
743 compatible with simple two-component mixtures in isotope variation diagrams (Pb, Sr, Nd and
744 Hf isotope ratios, see Labanieh et al., 2010). However, the cerium anomalies measured in the
745 same samples do not correlate with ϵ_{Nd} or ϵ_{Ce} values (Figure 11), even if samples that appear
746 to be significantly affected by fractional crystallization are discarded (see supplementary file
747 G). Samples from Bonin and Solomon Islands studied by Shimizu et al. (1992) show no
748 significant correlation in ϵ_{Nd} -Ce/Ce* and ϵ_{Ce} -Ce/Ce* diagrams (Figure 11), and, in a more
749 general way, there is a lack of correlation between ϵ_{Nd} - and Ce/Ce* in samples from the Izu-
750 Bonin arc (Hochstaedter et al., 2001). This strongly suggests that the cerium anomaly is not
751 always a good proxy of the sediment incorporation in the mantle wedge.

752 753 754 6. Conclusion

755
756 The measurement of $^{138}Ce/^{142}Ce$ and $^{143}Nd/^{144}Nd$ on 12 Mariana arc samples, 9 trench
757 sediments from ODP sites 800 and 801, 3 Mariana Trough Basalts and 3 MORB samples
758 provides new information regarding the LREE source of Mariana arc magmas and their
759 negative Ce anomalies. Since the back-arc basalt sample D68-2-1 is representative of the
760 local depleted mantle under the Mariana arc, it is used to model the depleted end-member in
761 the binary mixing calculations. The Ce-Nd binary mixing models were calculated using two
762 different enriched end-members: volcanoclastic sediments and biosiliceous sediments. Our
763 models show that a small proportion of a sedimentary melt derived from volcanoclastic
764 sediments (0.75% to 2.75%) must have been incorporated into the mantle source in order to
765 explain both $^{138}Ce/^{142}Ce$ and $^{143}Nd/^{144}Nd$ ratios of the arc samples and their negative Ce
766 anomalies (0.90 to 0.97). For biosiliceous samples, a too large proportion of a sedimentary
767 melt is required (up to 8%) to explain the Ce-Nd isotope composition of the lavas. Moreover
768 the incorporation of biosiliceous sediments generates too strong Ce anomalies. We highlight

1
2 770 the importance of using local materials, i.e. depleted mantle from the back-arc basin and
3
4 771 sediments from ODP sites 801 and 802, in the binary mixing calculations.

5
6 772 Other « magmatic » processes than partial melting and fractional crystallization, that
7
8 773 potentially affect Ce anomalies, have been also discussed: these are the influence of oxygen
9
10 774 fugacity on the change of valence state of Ce, the presence of residual accessory mineral
11
12 775 phases, or the involvement of aqueous fluids resulting from the dehydration of recycled
13
14 776 material. The proportion of Ce⁴⁺ for these redox conditions is extremely low. The precisions
15
16 777 on partition coefficient are not sufficient yet to attribute Ce anomaly variations in arc lavas to
17
18 778 one of these processes and more experiments are needed at different redox conditions. Their
19
20 779 influence on Ce/Ce* are limited in the Mariana arc context, nevertheless they cannot be totally
21
22 780 excluded for other arcs.

23
24 781

25
26 782 Comparing the whole database of ¹³⁸Ce/¹⁴²Ce data available for arc lavas reveals a
27
28 783 significant variability between arcs. Bonin and Solomon Island have εCe difficult to explain. A
29
30 784 better characterization of the local materials involved in their source together with a better
31
32 785 understanding of Ce, and more largely REE, behavior during magmatic processes, may help
33
34 786 understanding measured values. Turning to Martinique lavas, their Ce isotope compositions
35
36 787 can be explained by a binary mixing between depleted mantle and local sediments, but not
37
38 788 their Ce anomalies. So, the link between negative Ce anomalies and sediment additions has
39
40 789 to be made carefully and without globalizing the process to all subduction zones.

41
42 790

43
44 791

45 792 **Acknowledgements**

46
47
48 793 We would like to thank Matthias Willbold and Masaharu Tanimizu for providing us both the
49
50 794 Ce-AMES and the JMC-304 reference materials. Thanks to Pierre Schiano for the MORB
51
52 795 samples. Help in the chemistry lab provided by Chantal Bosq and with the mass
53
54 796 spectrometers by Delphine Auclair and Jean Luc Piro were highly valuable. The paper was
55
56 797 also improved by critical comments by W. White and an anonymous reviewer. This research
57
58 798 was financed by the French Government Laboratory of Excellence initiative n°ANR-10-LABX-

799 0006. This project has received funding from the European Union's Horizon 2020 research
800 and innovation programme under Grant Agreement N° 682778. This is Laboratory of
801 Excellence ClerVolc contribution number XXX.

802

803

804 **REFERENCES**

805 Aigner-Torres, M., Blundy, J., Ulmer, P., Pettke, T., 2007. Laser Ablation ICPMS study of trace element
806 partitioning between plagioclase and basaltic melts: An experimental approach. *Contrib. to*
807 *Mineral. Petrol.* 153, 647–667. doi:10.1007/s00410-006-0168-2

808 Allegre, C.J., Minster, J.F., 1978. Quantitative Models of Trace-Element Behavior in Magmatic
809 Processes. *Earth Planet. Sci. Lett.* 38, 1–25.

810 Amakawa, H., 1991. Isotopic compositions of Ce, Nd and Sr in ferromanganese nodules from the
811 Pacific and Atlantic Oceans, the Baltic and Barents Seas, and the Gulf of Bothnia *Earth Planet.*
812 *Sci. Lett.* 105, 554–565.

813 Avanzinelli, R., Prytulak, J., Skora, S., Heumann, a., Koetsier, G., Elliott, T., 2012. Combined 238U-
814 230Th and 235U- 231Pa constraints on the transport of slab-derived material beneath the
815 Mariana Islands. *Geochim. Cosmochim. Acta* 92, 308–328. doi:10.1016/j.gca.2012.06.020

816 Bartolini, A., Larson, R.L., 2001. Pacific microplate and the Pangea supercontinent in the Early to Middle
817 Jurassic. *Geology* 29, 735–738.

818 Bau, M., Schmidt, K., Koschinsky, a., Hein, J., Kuhn, T., Usui, a., 2014. Discriminating between
819 different genetic types of marine ferro-manganese crusts and nodules based on rare earth
820 elements and yttrium. *Chem. Geol.* 381, 1–9. doi:10.1016/j.chemgeo.2014.05.004

821 Bellot, N., Boyet, M., Doucelance, R., Pin, C., Chauvel, C., Auclair, D., 2015. Ce isotope systematics of
822 island arc lavas from the Lesser Antilles. *Geochim. Cosmochim. Acta* 168, 261–279.
823 doi:10.1016/j.gca.2015.07.002

824 Bézou, A., Humler, E., 2005. The Fe³⁺/ΣFe ratios of MORB glasses and their implications for mantle
825 melting. *Geochim. Cosmochim. Acta* 69, 711–725. doi:10.1016/j.gca.2004.07.026

826 Bouman, C., Elliott, T., Vroon, P.Z., 2004. Lithium inputs to subduction zones. *Chem. Geol.* 212, 59–79.
827 doi:10.1016/j.chemgeo.2004.08.004

828 Burnham, A.D., Berry, A.J., 2014. The effect of oxygen fugacity, melt composition, temperature and
829 pressure on the oxidation state of cerium in silicate melts. *Chem. Geol.* 366, 52–60.
830 doi:10.1016/j.chemgeo.2013.12.015

- 831 Burnham, A.D., Berry, A.J., 2012. An experimental study of trace element partitioning between zircon
832 and melt as a function of oxygen fugacity. *Geochim. Cosmochim. Acta* 95, 196–212.
833 doi:10.1016/j.gca.2012.07.034
- 834 Carpentier, M., 2007. Composition chimique des sédiments entrant dans la zone de subduction des
835 Petites Antilles. Thèse Université Joseph Fourier.
- 836 Carr, M.J., Feigenson, M.D., Bennett, E.A., 1990. Incompatible element and isotopic evidence for
837 tectonic control of source mixing and melt extraction along the Central American arc. *Contrib. to*
838 *Mineral. Petrol.* 105, 369–380. doi:10.1007/BF00286825
- 839 Chauvel, C., Blichert-Toft, J., 2001. A hafnium isotope and trace element perspective on melting of the
840 depleted mantle. *Earth Planet. Sci. Lett.* 190, 137–151. doi:10.1016/S0012-821X(01)00379-X
- 841 Chauvel, C., Bureau, S., Poggi, C., 2011. Comprehensive Chemical and Isotopic Analyses of Basalt and
842 Sediment Reference Materials. *Geostand. Geoanalytical Res.* 35, 125–143. doi:10.1111/j.1751-
843 908X.2010.00086.x
- 844 Chauvel, C., Marini, J.-C., Plank, T., Ludden, J.N., 2009. Hf-Nd input flux in the Izu-Mariana subduction
845 zone and recycling of subducted material in the mantle. *Geochemistry Geophys. Geosystems* 10,
846 1–23. doi:10.1029/2008GC002101
- 847 Cotten, J., Dez, A. Le, Bau, M., Caroff, M., Maury, R.C., Dulski, P., Fourcade, S., Bohn, M., Brousse, R.,
848 1995. Origin of anomalous rare-earth element and yttrium enrichments in subaerially exposed
849 basalts: Evidence from French Polynesia. *Chem. Geol.* 119, 115–138.
850 doi:http://dx.doi.org/10.1016/0009-2541(94)00102-E
- 851 Dixon, T.H., Batiza, R., 1979. Petrology and geochemistry of lavas in the northern Mariana: implications
852 for the origin of island arc basalts. *Contrib. to Mineral. Petrol.* 70, 167–181.
853 doi:10.1007/BF00374446
- 854 Doucelance, R., Bellot, N., Boyet, M., Hammouda, T., Bosq, C., 2014. What coupled cerium and
855 neodymium isotopes tell us about the deep source of oceanic carbonatites. *Earth Planet. Sci.*
856 *Lett.* 407, 175–186. doi:10.1016/j.epsl.2014.09.042
- 857 Eiler, J.M., Crawford, A., Elliott, T., Farley, K.A., Valley, J.W., Stolper, E.M., 2000. Oxygen Isotope
858 Geochemistry of Oceanic-Arc Lavas. *J. Petrol.* 41, 229–256. doi:10.1093/petrology/41.2.229
- 859 Eiler, J.M., Farley, K. a., Valley, J.W., Hauri, E., Craig, H., Hart, S.R., Stolper, E.M., 1997. Oxygen
860 isotope variations in ocean island basalt phenocrysts. *Geochim. Cosmochim. Acta* 61, 2281–
861 2293. doi:10.1016/S0016-7037(97)00075-6
- 862 Elderfield, H., Greaves, M.J., 1982. The rare earth elements in seawater. *Nature* 296, 214–219.
- 863 Elliott, T., Plank, T., Zindler, A., White, W., Bourdon, B., 1997. Element transport from slab to volcanic
864 front at the Mariana arc. *J. Geophys. Res.* 102, 14991. doi:10.1029/97JB00788

- 1
2
3
4
5
6
7
8
9
10
11
12
13
14
15
16
17
18
19
20
21
22
23
24
25
26
27
28
29
30
31
32
33
34
35
36
37
38
39
40
41
42
43
44
45
46
47
48
49
50
51
52
53
54
55
56
57
58
59
60
61
62
63
64
65
- 865 Elliott Tim, 1997. Fractionation of U and Th during mantle melting : a reprise. *Chem. Geol.* 139, 165–
866 183. doi:[http://dx.doi.org/10.1016/S0009-2541\(97\)00034-X](http://dx.doi.org/10.1016/S0009-2541(97)00034-X)
- 867 Ewart, A., Bryan, W.B., GILL, J.B., 1973. Mineralogy and Geochemistry of the Younger Volcanic Islands
868 of Tonga, S.W. Pacific. *J. Petrol.* 14, 429–465. doi:10.1093/petrology/14.3.429
- 869 Feigenson, M.D., Hofmann, A.W., Spera, F.J., 1983. Case studies on the origin of basalt. *Contrib. to*
870 *Mineral. Petrol.* 84, 390–405. doi:10.1007/BF01160290
- 871 Freymuth, H., Vils, F., Willbold, M., Taylor, R.N., Elliott, T., 2015. Molybdenum mobility and isotopic
872 fractionation during subduction at the Mariana arc. *Earth Planet. Sci. Lett.* 432, 176–186.
873 doi:10.1016/j.epsl.2015.10.006
- 874 Gale, A., Dalton, C.A., Langmuir, C.H., 2013. The mean composition of ocean ridge basalts 14, 489–
875 518. doi:10.1029/2012GC004334
- 876 Gribble, R.F., Stern, R.J., Bloomer, S.H., Stüben, D., O’Hearn, T., Newman, S., 1996. MORB mantle
877 and subduction components interact to generate basalts in the southern Mariana Trough back-
878 arc basin. *Geochim. Cosmochim. Acta* 60, 2153–2166. doi:[http://dx.doi.org/10.1016/0016-](http://dx.doi.org/10.1016/0016-7037(96)00078-6)
879 [7037\(96\)00078-6](http://dx.doi.org/10.1016/0016-7037(96)00078-6)
- 880 Gribble, R.F., Stern, R.J., Newman, S., Bloomer, S.H., O’Hearn, T., 1998. Chemical and Isotopic
881 Composition of Lavas from the Northern Mariana Trough: Implications for Magmagenesis in
882 Back-arc Basins. *J. Petrol.* 39, 125–154. doi:10.1093/etroj/39.1.125
- 883 Hamilton, P.J., O’Nions, R.K., Bridgwater, D., Nutman, A., 1983. Sm-Nd studies of Archaean
884 metasediments and metavolcanics from West Greenland and their implications for the Earth’s
885 early history. *Earth Planet. Sci. Lett.* 62, 263–272. doi:10.1016/0012-821X(83)90089-4
- 886 Hermann, J., Spandler, C.J., 2008. Sediment melts at sub-arc depths: An experimental study. *J. Petrol.*
887 49, 717–740. doi:10.1093/etrology/egm073
- 888 Hochstaedter, A., Gill J., Peters R., Broughton P., Holden P. and Taylor B., 2001. Across-arc
889 geochemical trends in the Izu-Bonin arc: contributions from the subducting slab. *Geochemistry*
890 *Geophys. Geosystems* 2, 1525-2027.
- 891 Hofmann, A., 1988. Chemical differentiation of the Earth: the relationship between mantle, continental
892 crust, and oceanic crust. *Earth Planet. Sci. Lett.* 90, 297–314.
- 893 Hole, M., Saunders, A., Marriner, G., Tarney, J., 1984. Subduction of Pelagic Sediments - Implications
894 for the Origin of Ce-Anomalous Basalts From the Mariana Islands 141, 453–472.
895 doi:10.1144/gsjgs.141.3.0453
- 896 Ishikawa, T., Nakamura, E., 1994. Origin of the slab component in arc lavas from across-arc variation of
897 B and Pb isotopes. *Nature* 370, 205–208. doi:10.1038/370205a0

- 898 Ishikawa, T., Tera, F., 1999. Two isotopically distinct fluid components involved in the Mariana Arc:
899 Evidence from Nb/B ratios and B, Sr, Nd, and Pb isotope systematics. *Geology* 27, 83–86.
- 900 Jakes, P., Gill, J., 1970. Rare earth elements and the island arc tholeiitic series. *Earth Planet. Sci. Lett.*
901 9, 17–28. doi:[http://dx.doi.org/10.1016/0012-821X\(70\)90018-X](http://dx.doi.org/10.1016/0012-821X(70)90018-X)
- 902 Johnson, M.C., Plank, T., 1999. Dehydration and melting experiments constrain the fate of subducted
903 sediments. *Geochemistry Geophys. Geosystems* 1, 1. doi:10.1029/1999GC000014
- 904 Karl, S.M., Wandless, G. a, Karpoff, a M., 1992. Sedimentological and geochemical characteristics of
905 Leg 129 siliceous deposits. . Larson R.L., Lancelot Y. al., Proc. ODP, Sci. Results, 129, Coll.
906 Station. TX (Ocean Drill. Program) 129, 31–79.
- 907 Karpoff, A.M., 1992. Cenozoic and Mesozoic sediments from the Pigafetta Basin, Leg 129, Sites 800
908 and 801: mineralogical and geochemical trends of the deposits overlying the oldest oceanic
909 crust. Proc. Ocean Drill. Program, Sci. Results 129, 3–30.
910 doi:doi:10.2973/odp.proc.sr.129.110.1992
- 911 Karpoff, A.M., France-Lanord, C., Lothe, F., Karcher, P., 1992. Miocene tuff from Mariana Basin, Leg
912 129, Site 802: a first deep-sea occurrence of thaumasite. Proc., Sci. results, ODP, Leg 129, old
913 Pacific crust 129, 119–135.
- 914 Kelley, K.A., Cottrell, E., 2009. Water and the oxidation state of subduction zone magmas. *Science* 325,
915 605–607. doi:<https://doi.org/10.1126/science.1174156>
- 916 Kelley, K.A., Plank, T., Newman, S., Stolper, E.M., Grove, T.L., Parman, S., Hauri, E.H., 2010. Mantle
917 Melting as a Function of Water Content beneath the Mariana Arc. *J. Petrol.* 51, 1711–1738.
918 doi:10.1093/petrology/egq036
- 919 Klemme, S., Prowatke, S., Hametner, K., Günther, D., 2005. Partitioning of trace elements between
920 rutile and silicate melts: Implications for subduction zones. *Geochim. Cosmochim. Acta* 69,
921 2361–2371. doi:10.1016/j.gca.2004.11.015
- 922 Kohut, E. and Savov, I. P., 2008. Mantle Heterogeneity in the Southern Mariana Trough Indicated
923 Through B and Sr Isotopic Systematics, *Eos Trans. AGU*, 89(53), Fall Meet. Suppl. Abstract
924 V31A-2110.
- 925 Koppers, A.A.P., Staudigel, H., Pringle, M.S., Wijbrans, J.R., 2003. Short-lived and discontinuous
926 intraplate volcanism in the South Pacific: Hot spots or extensional volcanism? *Geochemistry,*
927 *Geophys. Geosystems* 4, n/a--n/a. doi:10.1029/2003GC000533
- 928 Larson, R.L., Lancelot, Y., 1992. proceeding Ocean Drilling Program scientific results, 129.
929 doi:doi:10.2973/odp.proc.sr.129.
- 930 Lawrence, M. G., Greig, A., Collerson, K. D., & Kamber, B. S. (2006). Rare earth element and yttrium
931 variability in South East Queensland waterways. *Aquatic Geochemistry*, 12(1), 39-72.

- 1
2
3
4
5
6
7
8
9
10
11
12
13
14
15
16
17
18
19
20
21
22
23
24
25
26
27
28
29
30
31
32
33
34
35
36
37
38
39
40
41
42
43
44
45
46
47
48
49
50
51
52
53
54
55
56
57
58
59
60
61
62
63
64
65
- 932 Longerich, H.P., 1993. Oxychlorine ions in inductively coupled plasma mass spectrometry: Effect of
933 chlorine speciation as Cl⁻ and ClO₄⁻. *J. Anal. At. Spectrom.* 8, 439–444.
- 934 Luhr, J.F. Carmichael, I.S.E., 1980. The Colima volcanic complex, Mexico. I: post-caldera andesites
935 from Volcan Colima. *Contributions to Mineralogy and Petrology* 71: 343-372.
- 936 Makishima, A., Masuda, A., 1994. Ce isotope ratios of N-type MORB. *Chem. Geol.* 118, 1–8.
- 937 Makishima, A., Shimizu, H., Masuda, A., 1987. Precise Measurement of Cerium and Lanthanum isotope
938 ratios. *mass Spectrom.* 35.
- 939 Martindale, M., Skora, S., Pickles, J., Elliott, T., Blundy, J., Avanzinelli, R., 2013. High pressure phase
940 relations of subducted volcanoclastic sediments from the west pacific and their implications for the
941 geochemistry of Mariana arc magmas. *Chem. Geol.* 342, 94–109.
942 doi:10.1016/j.chemgeo.2013.01.015
- 943 McDonough, W., Sun, S. -s., 1995. The composition of the Earth. *Chem. Geol.* 120, 223–253.
- 944 McKenzie, D., O’Nions, R.K., 1991. Partial Melt Distributions from Inversion of Rare Earth Element
945 Concentrations. *J. Petrol.* 32, 1021–1091. doi:10.1093/petrology/32.5.1021
- 946 Meijer, A., 1976. Pb and Sr isotopic data bearing on the origin of volcanic rocks from the Mariana island-
947 arc system. *Geol. Soc. Am. Bull.* 87, 1358–1369. doi:10.1130/0016-
948 7606(1976)87<1358:PASIDB>2.0.CO;2
- 949 Meijer, A., Reagan, M., 1981. Petrology and geochemistry of the island of Sarigan in the Mariana Arc;
950 calc-alkaline volcanism in an oceanic setting. *Contrib. to Mineral. Petrol.* 77, 337–354.
- 951 Moiroud, M., Pucéat, E., Donnadieu, Y., Bayon, G., Guiraud, M., Voigt, S., Deconinck, J.-F., Monna, F.,
952 2015. Evolution of neodymium isotopic signature of seawater during the Late Cretaceous:
953 Implications for intermediate and deep circulation. *Gondwana Res.*
954 doi:http://dx.doi.org/10.1016/j.gr.2015.08.005
- 955 Moriguti, T., Nakamura, E., 1998. Across-arc variation of Li isotopes in lavas and implications for
956 crust/mantle recycling at subduction zones. *Earth Planet. Sci. Lett.* 163, 167–174.
957 doi:http://dx.doi.org/10.1016/S0012-821X(98)00184-8
- 958 Papike, J.J., Karner, J.M., Shearer, C.K., 2005. Comparative planetary mineralogy : Valence state
959 partitioning of Cr , Fe , Ti , and V among crystallographic sites in olivine , pyroxene , and spinel
960 from planetary basalts. *Am. Mineral.* 90, 277–290. doi:10.2138/am.2005.1779
- 961 Parkinson, I.J., Arculus, R.J., 1999. The redox state of subduction zones: Insights from arc peridotites.
962 *Chem. Geol.* 160, 409–423.
- 963 Pearce, J. a., Stern, R.J., Bloomer, S.H., Fryer, P., 2005. Geochemical mapping of the Mariana arc-
964 basin system: Implications for the nature and distribution of subduction components.
965 *Geochemistry, Geophys. Geosystems* 6. doi:10.1029/2004GC000895

- 966 Peate, D. W., Pearce, J. A., Hawkesworth, C. J., Colley, H., Edwards C., M., H., Hirose K. 1997.
1
2 967 Geochemical variations in Vanuatu arc lavas: the role of subducted material and a variable
3
4 968 mantle wedge composition. *J. Petrol.*, 10, 1331-1358.
- 5 969 Picard, S., Lécuyer, C., Barrat, J.A., Garcia, J.P., Dromart, G., Sheppard, S.M.F., 2002. Rare earth
6
7 970 element contents of Jurassic fish and reptile teeth and their potential relation to seawater
8
9 971 composition (Anglo-Paris Basin, France and England). *Chem. Geol.* 186, 1–16.
10
11 972 doi:10.1016/S0009-2541(01)00424-7
- 12 973 Pin, C., Santos Zaldueguit, J.F., 1997. Sequential separation of light rare-earth elements , thorium and
13
14 974 uranium by miniaturized extraction chromatography : Application to isotopic analyses of silicate
15
16 975 rocks. *Anal. Chim. Acta* 339, 79–89.
- 17
18 976 Plank, T., 2013. *The Chemical Composition of Subducting Sediments*, 2nd ed, Treatise on
19
20 977 *Geochemistry: Second Edition*. Elsevier Ltd. doi:10.1016/B978-0-08-095975-7.00319-3
- 21 978 Plank, T., Cooper, L.B., Manning, C.E., 2009. Emerging geothermometers for estimating slab surface
22
23 979 temperatures. *Nat. Geosci.* 2, 611–615. doi:10.1038/ngeo614
- 24
25 980 Plank, T., Langmuir, C.H., 1998. The chemical composition of subducting sediment and its
26
27 981 consequences for the crust and mantle. *Chem. Geol.* 145, 325–394. doi:10.1016/S0009-
28
29 982 2541(97)00150-2
- 30
31 983 Pourmand, A., Dauphas, N., Ireland, T.J., 2012. A novel extraction chromatography and MC-ICP-MS
32
33 984 technique for rapid analysis of REE, Sc and Y: Revising CI-chondrite and Post-Archean
34
35 985 Australian Shale (PAAS) abundances. *Chem. Geol.* 291, 38–54.
36
37 986 doi:10.1016/j.chemgeo.2011.08.011
- 38 987 Prytulak, J., Nielsen, S.G., Ionov, D.A., Halliday, A.N., Harvey, J., Kelley, K.A., Niu, Y.L., Peate, D.W.,
39
40 988 Shimizu, K., Sims, K.W.W., 2013a. The stable vanadium isotope composition of the mantle and
41
42 989 mafic lavas. *Earth Planet. Sci. Lett.* 365, 177–189. doi:10.1016/j.epsl.2013.01.010
- 43 990 Prytulak, J., Nielsen, S.G., Plank, T., Barker, M., Elliott, T., 2013b. Assessing the utility of thallium and
44
45 991 thallium isotopes for tracing subduction zone inputs to the Mariana arc. *Chem. Geol.* 345, 139–
46
47 992 149. doi:10.1016/j.chemgeo.2013.03.003
- 48
49 993 Prytulak, J., Sossi, P.A., Halliday, A.N., Plank, T., Savage, P.S., Woodhead, J.D., 2017. Stable
50
51 994 vanadium isotopes as a redox proxy in magmatic systems ? *geochemical Perspect. Lett.* 3, 75–
52
53 995 84. doi:10.7185/geochemlet.1708
- 54
55 996 Ribeiro, J.M., Stern, R.J., Kelley, K.A., Shaw, A.M., Martinez, F., Ohara, Y., 2015. Composition of the
56
57 997 slab-derived fluids released beneath the Mariana forearc: Evidence for shallow dehydration of
58
59 998 the subducting plate. *Earth Planet. Sci. Lett.* 418, 136–148. doi:10.1016/j.epsl.2015.02.018
- 60 999 Rollinson, H., 1993. *Using geochemical data: evaluation, presentation, interpretation*, longman gr. ed.

- 1000 Rubatto, D., Hermann, J., 2003. Zircon formation during fluid circulation in eclogites (Monviso, Western
1 Alps): Implications for Zr and Hf budget in subduction zones. *Geochim. Cosmochim. Acta* 67,
2 2173–2187. doi:10.1016/S0016-7037(02)01321-2
3
4 1002
5 1003 Salimullah, A.R.M., 1992. Volcaniclastic facies and sequences, Leg 129. *Proc. Ocean Drill. Program,*
6
7 1004 *Sci. Results* 129. doi:10.1029/138GM10
8
9 1005 Salters, V.J.M., Stracke, A., 2004. Composition of the depleted mantle. *Geochemistry, Geophys.*
10
11 1006 *Geosystems* 5. doi:10.1029/2003GC000597
12
13 1007 Savage, P.S., Georg, R.B., Armytage, R.M.G., Williams, H. M., Halliday, A.N., 2010. Silicon isotope
14
15 1008 homogeneity in the mantle. *Earth Planet. Sci. Lett.*, 295, 139-146.
16
17 1009 Savov, I.P., Ryan, J.G., D'Antonio, M., Fryer, P., 2007. Shallow slab fluid release across and along the
18
19 1010 Mariana arc-basin system: Insights from geochemistry of serpentized peridotites from the
20
21 1011 Mariana fore arc. *J. Geophys. Res. Solid Earth* 112. doi:10.1029/2006JB004749
22
23 1012 Savov, I.P., Ryan, J.G., D'Antonio, M., Kelley, K., Mattie, P., 2005. Geochemistry of serpentized
24
25 1013 peridotites from the Mariana Forearc Conical Seamount, ODP Leg 125: Implications for the
26
27 1014 elemental recycling at subduction zones. *Geochemistry, Geophys. Geosystems* 6, 1–24.
28
29 1015 doi:10.1029/2004GC000777
30
31 1016 Schiano, P., Birck, J., Alegre, C.J., 1997. Osmium-strontium-neodymium-lead 150, 363–379.
32
33 1017 Schiano, P., Monzier, M., Eissen, J.P., Martin, H., Koga, K.T., 2010. Simple mixing as the major control
34
35 1018 of the evolution of volcanic suites in the Ecuadorian Andes. *Contrib. to Mineral. Petrol.* 160, 297–
36
37 1019 312. doi:10.1007/s00410-009-0478-2
38
39 1020 Schreiber, H.D., 1987. An Electrochemical Series of Redox Couples in Silicate Melts: a review and
40
41 1021 applications to geochemistry. *J. Geophys. Res.* 92, 9225–9232. doi:10.1029/JB092iB09p09225
42
43 1022 Schreiber, H.D., Lauer, H. V., Thanyasiri, T., 1980. The redox state of cerium in basaltic magmas: an
44
45 1023 experimental study of iron-cerium interactions in silicate melts. *Geochim. Cosmochim. Acta* 44,
46
47 1024 1599–1612. doi:http://dx.doi.org/10.1016/0016-7037(80)90120-9
48
49 1025 Schuth S., Munker C., Konig S., Qopoto C., Basi S., Garde-Schonberg D and Ballaus C., 2009.
50
51 1026 Petrogenesis of lavas along the Solomon Island ARc, SW Pacific: Coupling of compositional
52
53 1027 variations and subduction Zone Geometry. *J. Petrol.* 50, 781-811.
54
55 1028 Seno, T., 1977. The instantaneous rotation vector of the Philippine Sea plate relative to the Eurasian
56
57 1029 plate. *Tectonophysics* 42, 209–226.
58
59 1030 Shimizu, H., Sawatari, H., Kawata, Y., Dunkley, P.N., Masuda, A., 1992. Ce and Nd isotope
60
61 1031 geochemistry on island arc volcanic rocks with negative Ce anomaly: existence of sources with
62
63 1032 concave REE patterns in the mantle beneath the Solomon and Bonin island arcs. *Contrib. to*
64
65 1033 *Mineral. Petrol.* 110, 242–252. doi:10.1007/BF00310741

- 1034 Skora, S., Blundy, J., 2012. Monazite solubility in hydrous silicic melts at high pressure conditions
1035 relevant to subduction zone metamorphism. *Earth Planet. Sci. Lett.* 321–322, 104–114.
1036 doi:10.1016/j.epsl.2012.01.002
- 1037 Skora, S., Freymuth, H., Blundy, J., Elliott, T., Guillong, M., 2017. An experimental study of the
1038 behaviour of cerium / molybdenum ratios during subduction : Implications for tracing the slab
1039 component in the Lesser Antilles and Mariana Arc. *Geochim. Cosmochim. Acta* 212, 133–155.
1040 doi:10.1016/j.gca.2017.05.025
- 1041 Smythe, D.J., Brenan, J.M., 2016. Magmatic oxygen fugacity estimated using zircon-melt partitioning of
1042 cerium. *Earth Planet. Sci. Lett.* 453, 260–266. doi:10.1016/j.epsl.2016.08.013
- 1043 Smythe, D.J., Brenan, J.M., 2015. Cerium Oxidation State in Silicate Melts: Combined fO₂, Temperature
1044 and Compositional Effects. *Geochim. Cosmochim. Acta*.
1045 doi:http://dx.doi.org/10.1016/j.gca.2015.07.016
- 1046 Snyder, G.T., Savov, I. P., Muramatsu, Y., 2004. Iodine and boron in Mariana serpentine mud volcanoes
1047 (ODP 125 and 195): Implications for forearc processes and subduction recycling, In Shinohara,
1048 M., Salisbury, M.H., and Richter, C. (Eds.), *Proc. ODP, Sci. Results*, 195
- 1049 Stern, R.J., Fouch, M.J., Klemperer, S.L., 2003. An overview of the Izu-Bonin-Mariana subduction
1050 factory. *Insid. subduction Fact., Geophysical Monograph*. doi:10.1029/138GM10
- 1051 Stolper, E., Newman, S., 1994. The role of water in the petrogenesis of Mariana trough magmas. *Earth*
1052 *Planet. Sci. Lett.* 121, 293–325. doi:10.1016/0012-821X(94)90074-4
- 1053 Straub, S.M., 2003. The evolution of the Izu Bonin - Mariana volcanic arcs (NW Pacific) in terms of
1054 major element chemistry. *Geochemistry, Geophys. Geosystems* 4, 1–33.
1055 doi:10.1029/2002GC000357
- 1056 Syracuse, E.M., Abers, G.A., 2006. Global compilation of variations in slab depth beneath arc volcanoes
1057 and implications. *Geochemistry, Geophys. Geosystems* 7, n/a--n/a. doi:10.1029/2005GC001045
- 1058 Syracuse, E.M., van Keken, P.E., Abers, G.A., 2010. The global range of subduction zone thermal
1059 models. *Phys. Earth Planet. Inter.* 183, 73–90. doi:10.1016/j.pepi.2010.02.004
- 1060 Tanaka, T., Togashi, S., Kamioka, H., Amakawa, H., Kagami, H., Hamamoto, T., Yuhara, M., Orihashi,
1061 Y., Yoneda, S., Shimizu, H., Kunimaru, T., Takahashi, K., Yanagi, T., Nakano, T., Fujimaki, H.,
1062 Shinjo, R., Asahara, Y., Tanimizu, M., Dragusanu, C., 2000. JNdi-1: a neodymium isotopic
1063 reference in consistency with LaJolla neodymium, *Chemical Geology*. doi:10.1016/S0009-
1064 2541(00)00198-4
- 1065 Tanimizu, M., 2000. Geophysical determination of the ¹³⁸La β- decay constant. *Phys. Rev.* 62, 140–
1066 143.

- 1067 Taylor, B., Martinez, F., 2003. Back-arc basin basalt systematics. *Earth Planet. Sci. Lett.* 210, 481–497.
1068 doi:10.1016/S0012-821X(03)00167-5
- 1069 Tollstrup, D.L., Gill, J.B., 2005. Hafnium systematics of the Mariana arc: Evidence for sediment melt and
1070 residual phases. *Geology* 33, 737–740. doi:10.1130/G21639.1
- 1071 Trail, D., Watson, E.B., Tailby, N.D., 2011. The oxidation state of Hadean magmas and implications for
1072 early Earth's atmosphere. *Nature* 480, 79-U238. doi:10.1038/nature10655
- 1073 Tsay, A., Zajacz, Z., Ulmer, P., Sanchez-Valle, C., 2017. Mobility of major and trace elements in the
1074 eclogite-fluid system and element fluxes upon slab dehydration. *Geochim. Cosmochim. Acta*
1075 198, 70–91. doi:10.1016/j.gca.2016.10.038
- 1076 Vervoort, J.D., Plank, T., Prytulak, J., 2011a. The Hf-Nd isotopic composition of marine sediments.
1077 *Geochim. Cosmochim. Acta* 75, 5903–5926. doi:10.1016/j.gca.2011.07.046
- 1078 Vervoort, J.D., Plank, T., Prytulak, J., 2011b. The Hf–Nd isotopic composition of marine sediments.
1079 *Geochim. Cosmochim. Acta* 75, 5903–5926. doi:10.1016/j.gca.2011.07.046
- 1080 Volpe, A.M., Douglas Macdougall, J., Hawkins, J.W., 1987. Mariana Trough basalts (MTB): trace
1081 element and SrNd isotopic evidence for mixing between MORB-like and Arc-like melts. *Earth*
1082 *Planet. Sci. Lett.* 82, 241–254. doi:10.1016/0012-821X(87)90199-3
- 1083 Voegelin, A. R., Pettke, T., Greber, N. D., von Niederhäusern, B., & Nægler, T. F., 2014. Magma
1084 differentiation fractionates Mo isotope ratios: evidence from the Kos Plateau Tuff (Aegean Arc).
1085 *Lithos*, 190, 440-448.
- 1086 von Huene, R., Scholl, D.W., 1991. Observations at convergent margins concerning sediment
1087 subduction, subduction erosion, and the growth of continental crust. *Rev. Geophys.* 29, 279.
1088 doi:10.1029/91RG00969
- 1089 Vroon, P.Z., Bergen, M.J. van, Klaver, G.J., White, W.M., 1995. Strontium, neodymium, and lead
1090 isotopic and trace-element signatures of the {East} Indonesian sediments: provenance and
1091 implications for banda arc magma genesis. *Geochim. Cosmochim. Acta* 59, 2573–2598.
1092 doi:http://dx.doi.org/10.1016/0016-7037(95)00151-4
- 1093 Wade, J. a., Plank, T., Stern, R.J., Tollstrup, D.L., Gill, J.B., O'Leary, J.C., Eiler, J.M., Moore, R.B.,
1094 Woodhead, J.D., Trusdell, F., Fischer, T.P., Hilton, D.R., 2005. The May 2003 eruption of
1095 Anatahan volcano, Mariana Islands: Geochemical evolution of a silicic island-arc volcano. *J.*
1096 *Volcanol. Geotherm. Res.* 146, 139–170. doi:10.1016/j.jvolgeores.2004.11.035
- 1097 Williams, H.M., Prytulak, J., Woodhead, J.D., Kelley, K.A., Brounce, M., Plank, T., 2018. Interplay of
1098 crystal fractionation, sulfide saturation and oxygen fugacity on the iron isotope composition of arc
1099 lavas: an example from the Marianas. *Geochim. Cosmochim. Acta*, 226, 224-243.
- 1100

- 1101 White, W.M., Dupré, B., 1986. Sediment subduction and magma genesis in the Lesser Antilles: isotopic
1102 and trace element constraints. *J. Geophys. Res. Solid Earth* 91, 5927–5941.
1103 doi:10.1029/JB091iB06p05927
- 1104 White, W.M., Patchett, J., 1984. HfNdSr isotopes and incompatible element abundances in island arcs:
1105 implications for magma origins and crust-mantle evolution. *Earth Planet. Sci. Lett.* 67, 167–185.
1106 doi:10.1016/0012-821X(84)90112-2
- 1107 Willbold M. (2007) Determination of Ce isotopes by TIMS and MC-ICPMS and initiation of a new,
1108 homogeneous Ce isotopic reference material. *J. Anal. At. Spectrom.* 22(22), 1364–1372.
1109 doi:10.1039/b705306a
- 1110 Willig, M., and Stracke, A., (2018) Accurate and precise measurement of Ce isotope ratios by thermal
1111 ionization mass spectrometry (TIMS). *Chemical Geology*, 476, 119-129.
- 1112 Woodhead, J., Eggins, S., Gamble, J., 1993. High field strength and transition element systematics in
1113 island arc and back-arc basin basalts: Evidence for multi-phase melt extraction and a depleted
1114 mantle wedge. *Earth Planet. Sci. Lett.* 114, 491–504. doi:10.1016/0012-821X(93)90078-N
- 1115 Woodhead, J., Stern, R.J., Pearce, J., Hergt, J., Vervoort, J., 2012. Hf-Nd isotope variation in Mariana
1116 Trough basalts: The importance of “ambient mantle” in the interpretation of subduction zone
1117 magmas. *Geology* 40, 539–542. doi:10.1130/G32963.1
- 1118 Woodhead, J.D., 1989. Geochemistry of the Mariana arc (western Pacific): Source composition and
1119 processes. *Chem. Geol.* 76, 1–24. doi:10.1016/0009-2541(89)90124-1
- 1120 Woodhead, J.D., 1988. The origin of geochemical variations in Mariana lavas: A general model for
1121 petrogenesis in intra-oceanic island arcs? *J. Petrol.* 29, 805–830. doi:10.1093/petrology/29.4.805
- 1122 Woodhead, J.D., Fraser, D.G., 1985. Pb, Sr and 10Be isotopic studies of volcanic rocks from the
1123 Northern Mariana Islands. Implications for magma genesis and crustal recycling in the Western
1124 Pacific. *Geochim. Cosmochim. Acta* 49, 1925–1930. doi:http://dx.doi.org/10.1016/0016-
1125 7037(85)90087-0
- 1126 Workman, R.K., Hart, S.R., 2005. Major and trace element composition of the depleted MORB mantle
1127 (DMM). *Earth Planet. Sci. Lett.* 231, 53–72. doi:10.1016/j.epsl.2004.12.005

1128
1129
1130
1131
1132

Figure captions

1133 Figure 1: Bathymetric map of the Mariana arc showing the location of the samples analyzed in
1134 this study. Blue triangles: arc volcanoes; red circles: Mariana Trough (backarc) basalts; and
1135 white squares: ODP drilling sediment sites from Leg 129 (800, 801 and 802). The basemap is
1136 from GeoMapApp (www.geomapapp.org).

1137
1138 Figure 2: Stratigraphic log of site 801 from ODP Leg 129 and the associated Ce anomaly
1139 (Ce/Ce^*) in function of depth (meters below sea level). Ce anomalies are calculated from data
1140 published in Karl et al. (1992) and Plank and Langmuir (1998) measured by INAA and
1141 ICPMS, respectively. The red arrows indicate the provenance of each studied sedimentary
1142 sample (Karl et al., 1992; Karpof, 1992; Salimullah, 1992).

1143
1144 Figure 3: Ce/Ce^* of studied lava samples from Mariana arc relative to (A) ϵ_{Nd} and (B) ϵ_{Ce} .
1145 Epsilon Ce values correspond to the weighted mean value when measurements have been
1146 duplicated. The error bar at the top of the diagram corresponds to the 2S.D. value determined
1147 on repeated standard measurements (40 ppm for ϵ_{Ce} and 9 ppm for ϵ_{Nd}). Deep blue triangle
1148 = Guguan; light blue triangle = Alamagan; orange triangle = Pagan; black triangle = Agrigan;
1149 grey triangle = Sagrigan; green triangle = Ascuncion; white triangle = Uracas.

1150
1151 Figure 4: REE patterns of the three studied Mariana Trough basalts normalized to CI-
1152 chondrite (McDonough and Sun, 1995). The N-MORB from Hofmann (1988) is shown for
1153 comparison (black line). Sample D68-2-1 is depleted in Light REE and follows the same
1154 pattern as N-MORB, whereas C7 and D3-2-1 are enriched in LREE.

1155
1156 Figure 5: A) ϵ_{Ce} vs ϵ_{Nd} values for MTB (red diamonds), Pacific MORB (orange circles),
1157 Mariana arc samples (blue triangles) and biosiliceous sediments (green squares). The 2SD
1158 for ϵ_{Ce} and ϵ_{Nd} illustrates the external reproducibility on repeated measurements of AMES
1159 and JNdi-1 standards. The two curves correspond to binary mixing between the Mariana
1160 Trough basalt D68-2-1 and components derived from biosiliceous sediments D68-801B33R

1161 and D68-801A17R that show the most extreme ϵ_{Ce} values. The white stars indicate the
1162 sedimentary proportions needed to explain the Ce and Nd isotopic compositions of the
1163 volcanic arc samples. Similar results are obtained using a «mean» sedimentary component
1164 (supplementary information). B) Evolution of the modeled Ce/Ce* with respect to the
1165 sedimentary proportions determined using the binary mixing models in Figure 5A. The white
1166 dots corresponds to Ce/Ce* calculated for 2.5% to 8% of sedimentary products at the lava
1167 source. The modeled Ce anomalies can be compared with the Ce/Ce* range in the Mariana
1168 arc samples represented in the right part of the figure B. Input parameters of the models are
1169 given in Table 3.

1171 Figure 6 A) ϵ_{Ce} vs ϵ_{Nd} values for MTB (red diamonds), Pacific MORB (orange circles),
1172 Mariana arc samples (blue triangles) and volcanoclastic sediments (purple squares). The 2SD
1173 in ϵ_{Ce} and ϵ_{Nd} illustrates the external reproducibility on repeated measurements of AMES and
1174 JNdi-1 standards. The two curves correspond to binary mixing between the Mariana Trough
1175 basalt D68-2-1 and components derived from volcanoclastic sediments (samples 801B-8R3
1176 and 801B-7R which $^{138}\text{Ce}/^{142}\text{Ce}$ compositions are the two most extreme) as enriched end-
1177 members. The white stars indicate the sedimentary proportions allowing to reproduce the Ce
1178 and Nd isotopic compositions of the arc lavas with melt products from volcanoclastic
1179 sediments in their source. Similar results are obtained using a «mean» sedimentary
1180 component (supplementary information). B) Evolution of the modeled Ce/Ce* with respect to
1181 the sedimentary proportions. The white dots correspond to Ce/Ce* calculated for 0.75% to
1182 2.75% of sedimentary products at the lava source. The modeled Ce anomalies can be
1183 compared with the Ce/Ce* range in the Mariana arc samples represented in the right part of
1184 the figure B. Input parameters of the models are given in Table 3.

1186 Figure 7: Dispersion of Ce anomalies (Ce/Ce*) in arc samples from many different subduction
1187 zones. All data are from the Georoc database (convergent margins data, <http://georoc.mpch-mainz.gwdg.de>). Ce/Ce* are calculated using $\text{Ce/Ce}^* = \text{Ce}_N / (\text{La}_N^{0.5} \times \text{Pr}_N^{0.5})$.

1190 Figure 8: Evolution of Ce/Ce* anomaly during (A) batch melting and (B) fractional
1191 crystallization. The $\Delta\text{Ce}/\text{Ce}^*$ represents the Ce/Ce* of the melt subtracted to the Ce/Ce* of
1192 the initial solid/melt (100% of melting in A and 100% of liquid in B). To produce diagram A, we
1193 considered 2 modal compositions: a garnet peridotite (55% ol, 25% opx, 11% cpx, 9% grt,
1194 black line) and a spinel-garnet peridotite (55% ol, 25% opx, 11% cpx, 6% grt, 3% sp; grey
1195 line). We also used the sedimentary proportions involved in the magma genesis defined from
1196 Ce-Nd isotopes: 2% of melt extracted from volcanoclastic sediments (Mariana) and 5% fluids
1197 coming from the partial melting of the GLOSS-II reservoir (Martinique). The fluid composition
1198 was calculated by applying the bulk solid/fluid partition coefficients measured from the
1199 experiments carried out by Martindale et al. (2013) for Mariana and by Johnson and Plank
1200 (1999) for Lesser Antilles. Light REE concentrations of the mantle source are those proposed
1201 by Salters and Stracke (2004) for the depleted mantle. The bulk partition coefficients (D) of
1202 the garnet-spinel peridotite are K_D values of McKenzie and O'Nions (1991). $\Delta\text{Ce}/\text{Ce}^*$ values
1203 are identical whatever the sediment proportions and the nature of the sediments showing that
1204 only the mineralogy of the mantle wedge changes the cerium anomaly of the produced melt.
1205 In diagram B, the blue line corresponds to the Mariana and the red field to Martinique. The
1206 crystallizing mineral assemblage is 48.6% plagioclase, 35.9% clinopyroxene, 1.1%
1207 orthopyroxene, 7.3% olivine and 7.1% magnetite (Table 5 in Dixon and Batiza, 1979) for
1208 Mariana, whereas a range of compositions has been tested for Martinique andesites using the
1209 propositions made in Labanieh et al. (2012): 45-50% plagioclase, 30-45% hornblende, 7-10%
1210 orthopyroxene, 3-5% clinopyroxene, 0-5% garnet. The initial magmas are similar to those
1211 produced by 10% of partial melting in figure A.

1212
1213 Figure 9: Th/Nd vs Nd for (A) Mariana lavas and (B) Martinique lavas. For the Mariana
1214 samples, Th and Nd concentrations are from Elliott et al. (1997) and from this study,
1215 respectively. Nd and Th concentrations for Martinique lavas are from Labanieh et al. (2012).
1216 The box represents a schematic C^H/C^M versus C^H diagram, where C^H and C^M are the
1217 concentrations of a highly incompatible element and of a moderately incompatible one
1218 (Schiano et al., 2010). A fit forming a near-horizontal line indicates a fractional crystallization

1219 process whereas a positive straight line fit indicates a partial melting process (Allègre and
1220 Minster, 1978; Feigenson et al., 1983).

1221

1222 Figure 10: Compilation of ϵ_{Ce} vs ϵ_{Nd} data for samples from arc setting including lavas and
1223 sediments and mid-ocean ridge basalts. Salomon and Bonin island data are from Shimizu et
1224 al. (1992) and $^{138}\text{Ce}/^{142}\text{Ce}$ ratios are normalized using JMC-304 data (Bellot et al., 2015;
1225 Shimizu et al., 1992). Martinique lavas, sediments from DSDP site 144 and a few MORBs are
1226 from Bellot et al., (2015). MORB data from Makishima and Masuda (1994) have $^{138}\text{Ce}/^{142}\text{Ce}$
1227 ratios normalized with BCR-1 and BCR-2.

1228

1229 Figure 11: (A) ϵ_{Nd} vs Ce/Ce^* and (B) ϵ_{Ce} vs Ce/Ce^* for arc settings volcanic rocks. Data from
1230 this study and literatures values (Martinique in Bellot et al., 2015 and Labanieh et al., 2010,
1231 2012; Bonin and Salomon from Shimizu et al., 1992). The Ce/Ce^* is determined by
1232 logarithmic interpolation of La and Pr.

1233

1234

1235

1236 **Table captions**

1237

1238 Table1: SiO_2 (wt %) and Rare Earth Element concentrations (ppm) for Mariana lavas,
1239 sediments from ODP sites 801 and 802, Mariana Trough Basalts and Pacific MORB. All SiO_2
1240 data are from literature (Bézos and Humler, 2005; Elliott et al., 1997; Karl et al., 1992; Karpof,
1241 1992; Karpoff et al., 1992; Pearce et al., 2005; Schiano et al., 1997; Vervoort et al., 2011).
1242 REE data were measured in this study by Inductively Coupled Plasma Mass Spectrometer
1243 (ICP-MS; quadrupole Agilent 7500) for the following samples: Mariana lavas, 4 of the
1244 sediments (802A-19R and 802A-43R, 801B-12R and 801B-7R), Mariana Trough Basalts and
1245 Searise 1 DR05 MORB. The analytical precision obtained on 4 repeated measurements of
1246 the BIR standard (2SD) varies for each element and is between 0.74% (Nd) to 4.06% (Eu). All
1247 the other REE data (sediments from sites 800 and 801, Cyana CY82 and Clipperton DR01
1248 MORB), in italic font, are from the literature. Sediments from ODP sites 801A and 801B are

1249 from Vervoort et al. (2011); two of the Pacific MORB's REE concentrations are from Gale et
1250 al. (2013).

1251

1252 Table 2: Results of $^{138}\text{Ce}/^{142}\text{Ce}$ and $^{143}\text{Nd}/^{144}\text{Nd}$ isotopic ratios for Mariana arc samples,
1253 sediments from ODP 801 and 802, Mariana Trough Basalts and Pacific MORB. The number
1254 of the analytical session is given. Some samples have been measured two or three times
1255 during the same analytical session (except for D68-2-1 which was in two different sessions).
1256 In these cases, the weighted mean value of both run (or all) is considered. (BS) is for
1257 biosiliceous sediments and (Volc) for volcanoclastic turbidites. The internal errors are 2s.e (2
1258 times the standard deviation divided by \sqrt{N} where N is the number of cycles). The $^{138}\text{Ce}/^{142}\text{Ce}$
1259 and $^{143}\text{Nd}/^{144}\text{Nd}$ ratios are also expressed in ϵ -notations normalized to CHUR values of
1260 0.0225654 (Bellot et al., 2015) and 0.512630 (Bouvier et al., 2008), respectively.

1261 $\epsilon = \left(\left(\frac{^{138}\text{Ce}/^{142}\text{Ce}_{\text{sample}}}{^{138}\text{Ce}/^{142}\text{Ce}_{\text{CHUR}}} - 1 \right) \times 10,000 \right); \quad \left(\left(\frac{^{143}\text{Nd}/^{144}\text{Nd}_{\text{sample}}}{^{143}\text{Nd}/^{144}\text{Nd}_{\text{CHUR}}} - \right.$
1262 $1 \right) \times 10,000$;

1263
1264 Table 3: Input parameters used to calculate the mixing curves presented in Figures 7, 8 and
1265 9. For the depleted end-member the concentrations are those of the DMM published by
1266 Salters and Stracke (2004) with a modified La concentration (from 0.234 to 0.265, see text).
1267 The concentrations of the two enriched end-members are those of the average sediments
1268 multiplied by the enrichment factors defined from experimental studies (Johnson and Plank
1269 (1999) for biosiliceous sediments, and from Martindale et al. (2013) for volcanoclastic ones.
1270 The ϵ_{Ce} and ϵ_{Nd} of each end-member are those measured in the samples. The ϵ_{Ce} and ϵ_{Nd} of
1271 the depleted end-member are from D68-2-1 Mariana Trough Basalt. Ce/Ce* corresponds to
1272 logarithmic calculations between La and Pr.

1273 ^a The enrichment factor is the ratio of element concentration in fluids over element
1274 concentration in the solid starting bulk: $C_{\text{fluid}}/C_{\text{starting bulk}}$.

1275

Figure

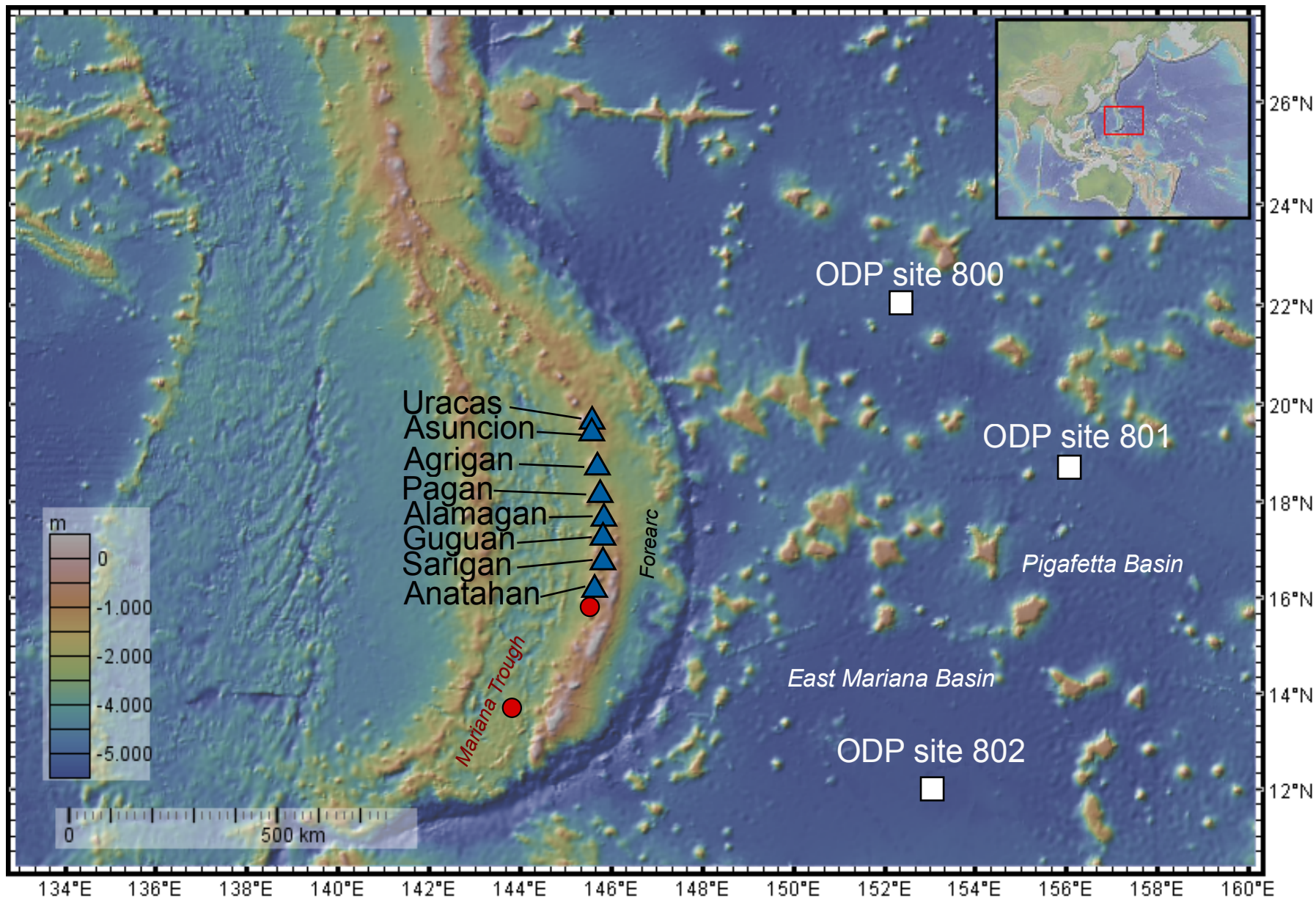


Figure 1 Bellot et al.

Site 801

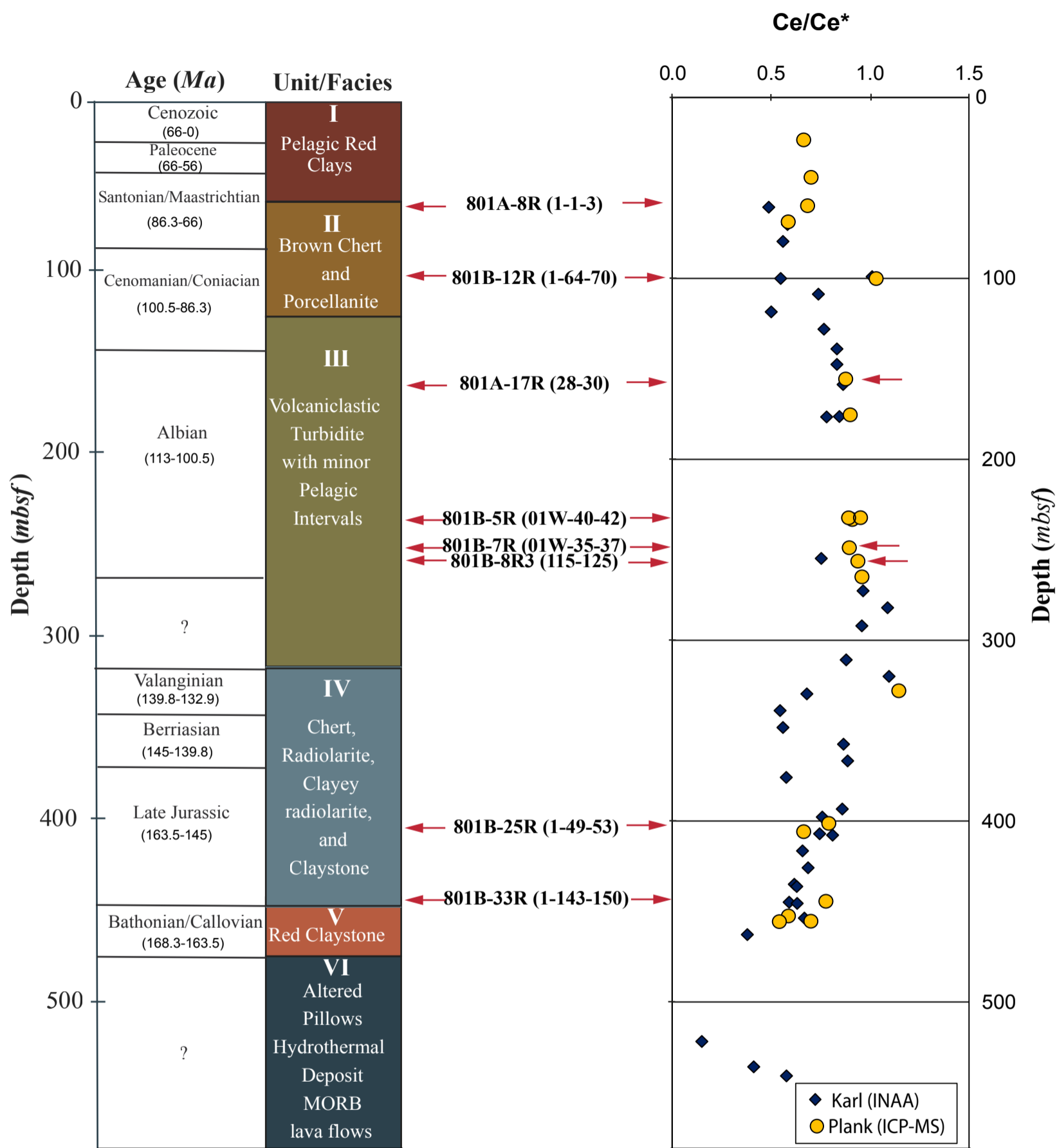


Figure 2 Bellot et al.

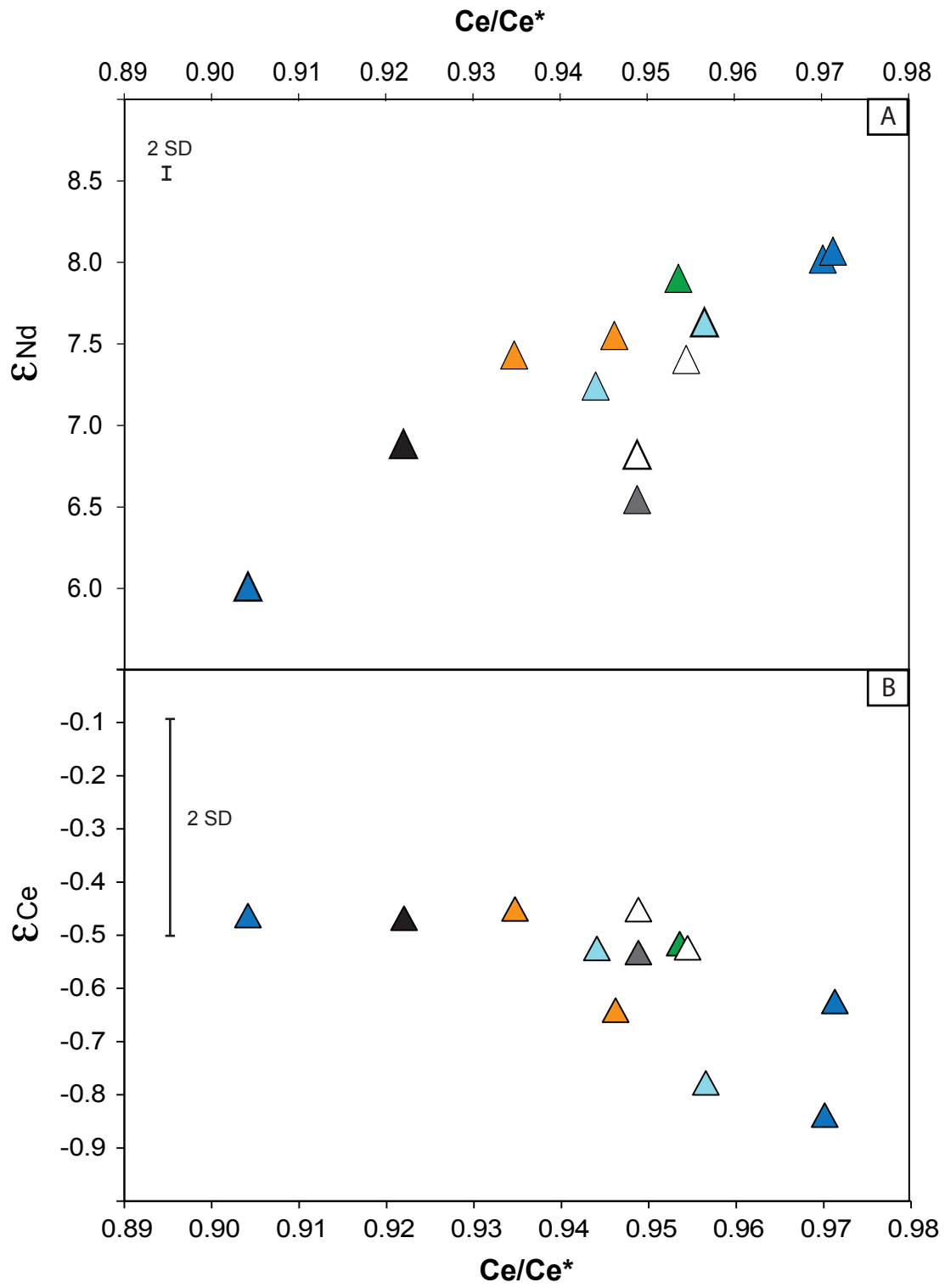


Figure 3. Bellot et al.

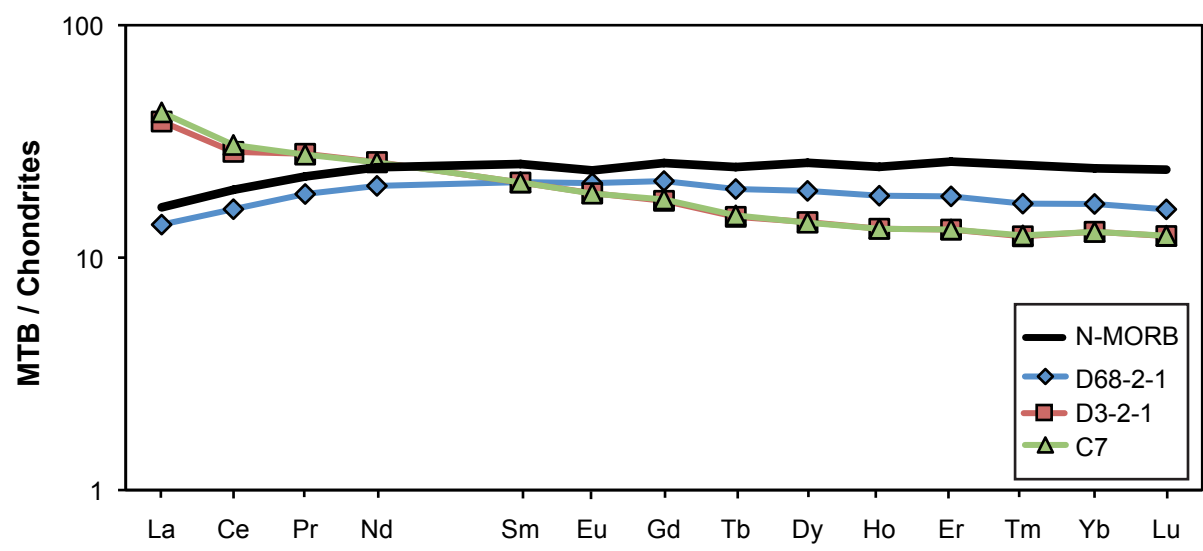


Figure 4. Bellot et al.

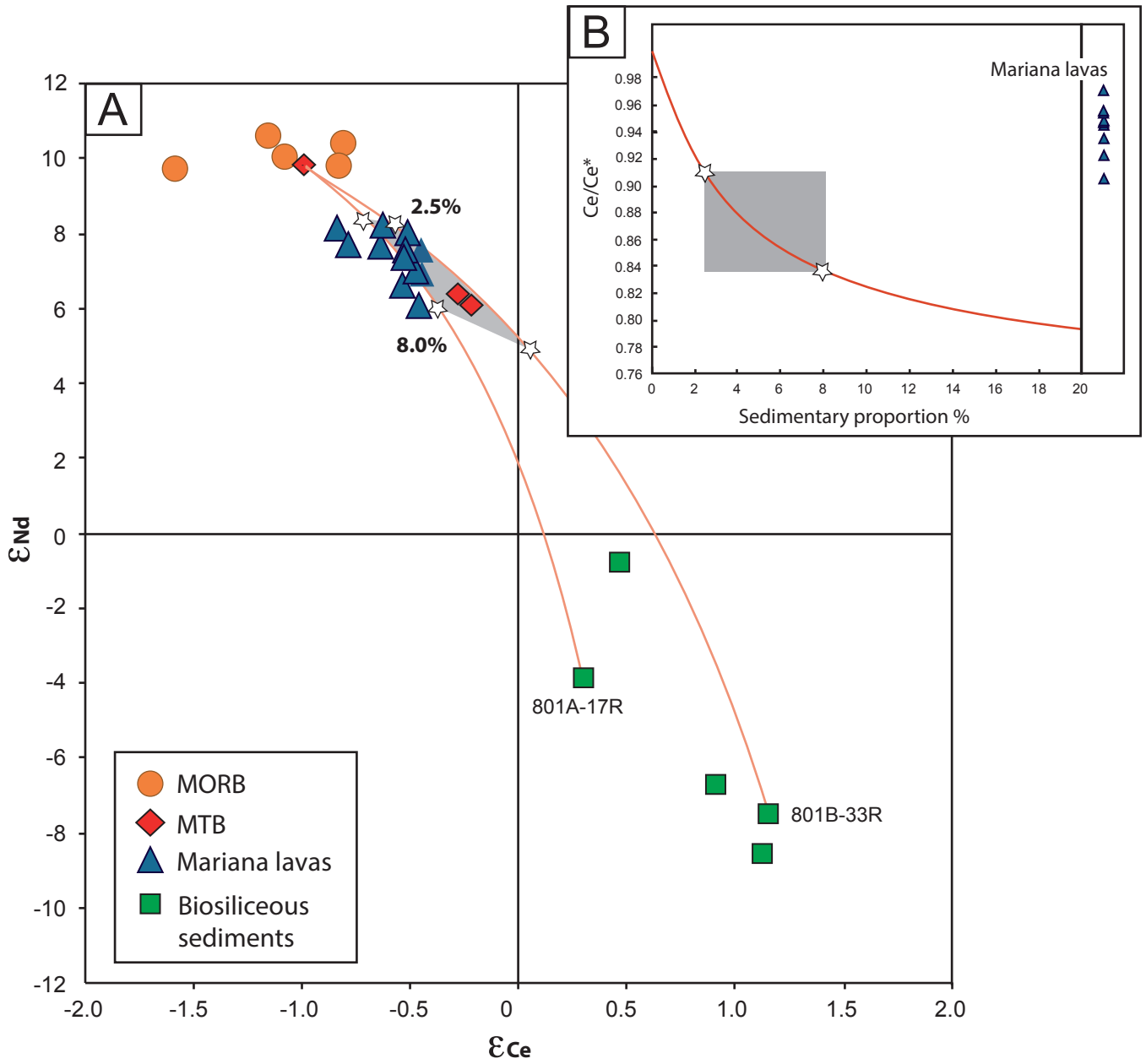


Figure 5. Bellot et al.

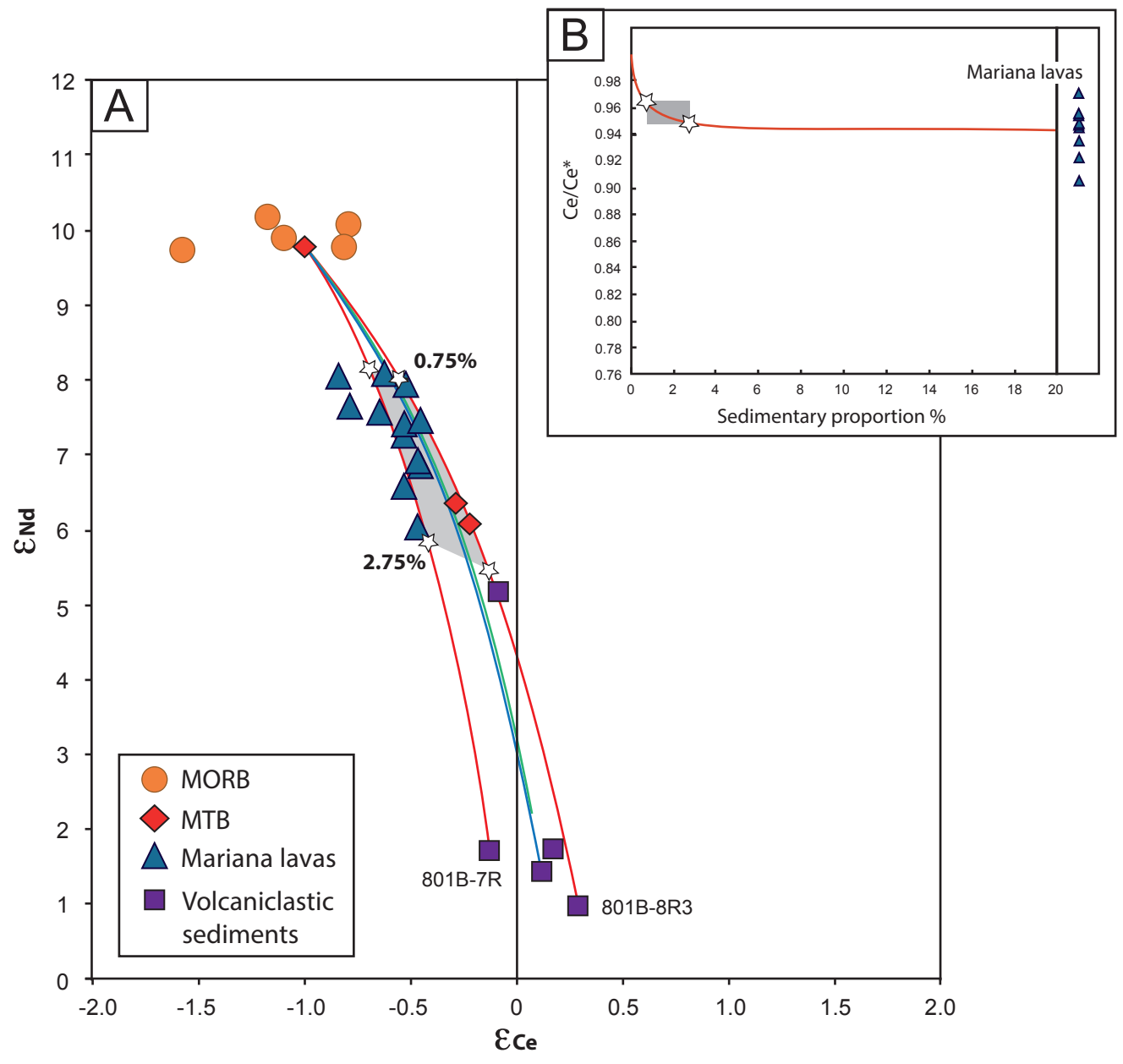


Figure 6. Bellot et al.

Figure

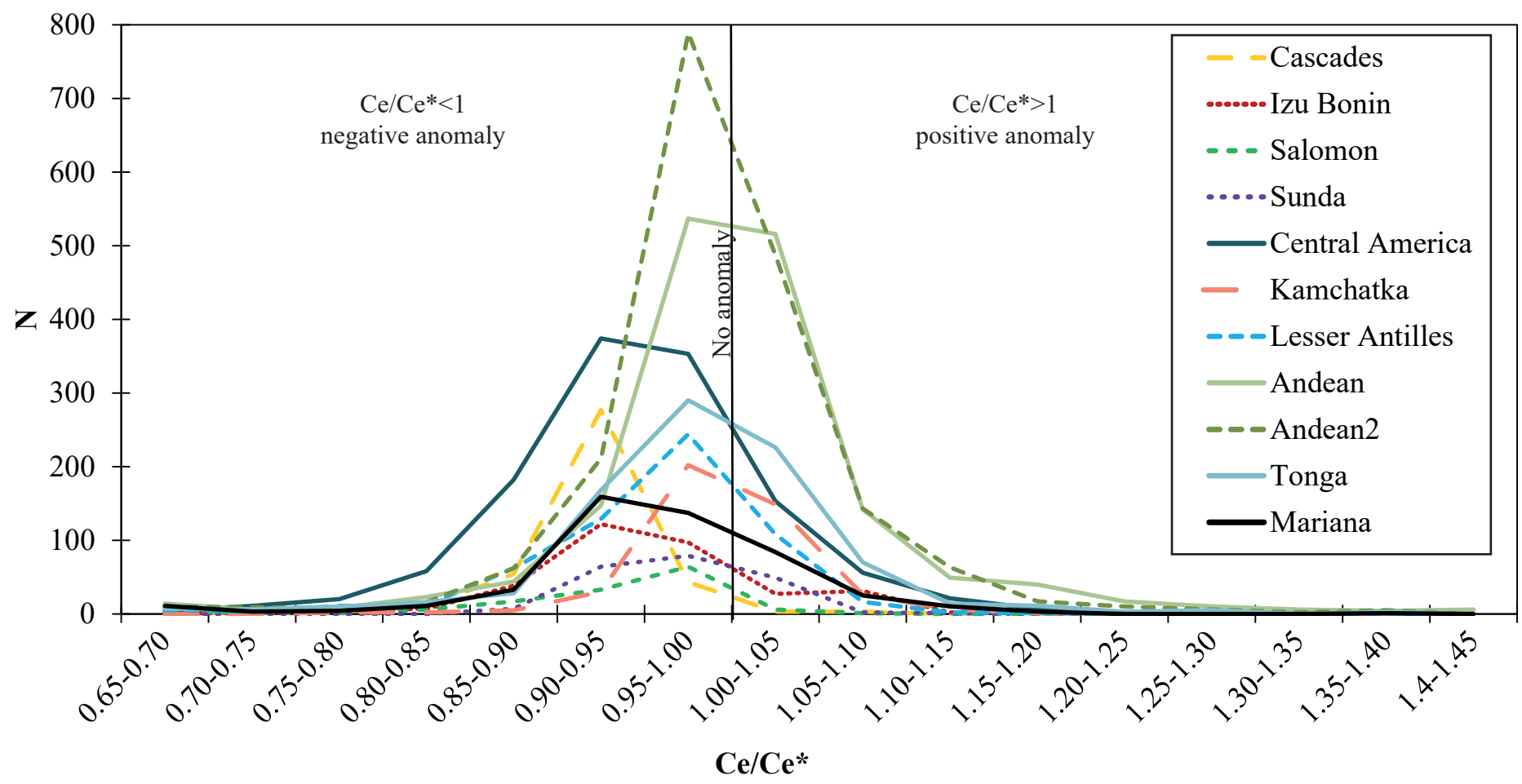


Figure 7 Bellot et al.

Figure

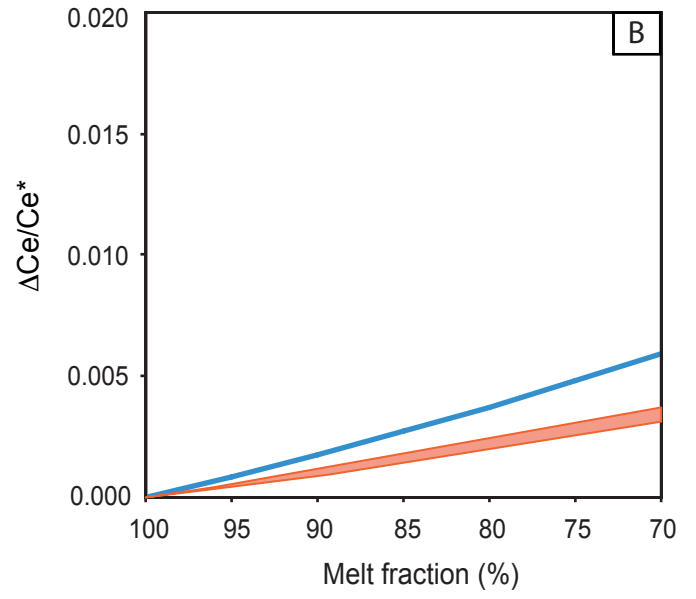
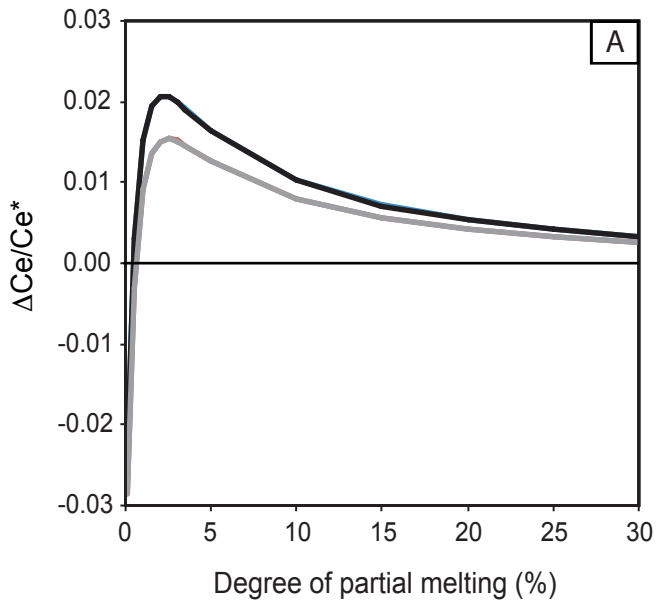


Figure 8. Bellot et al.

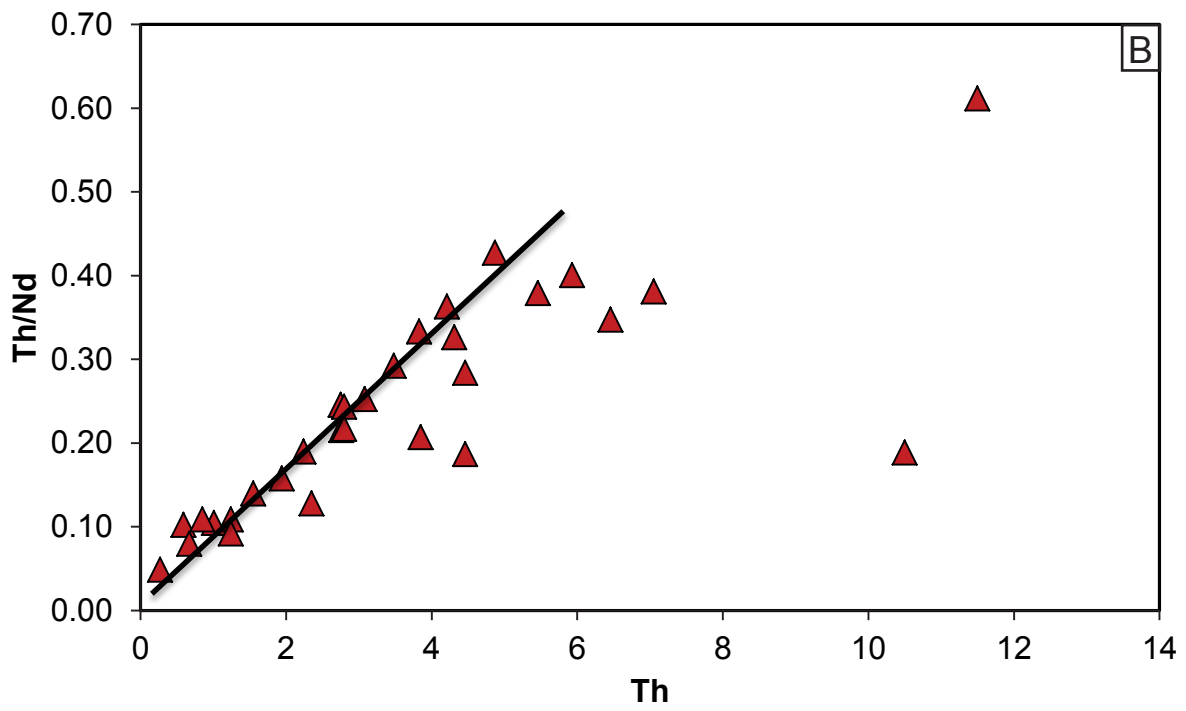
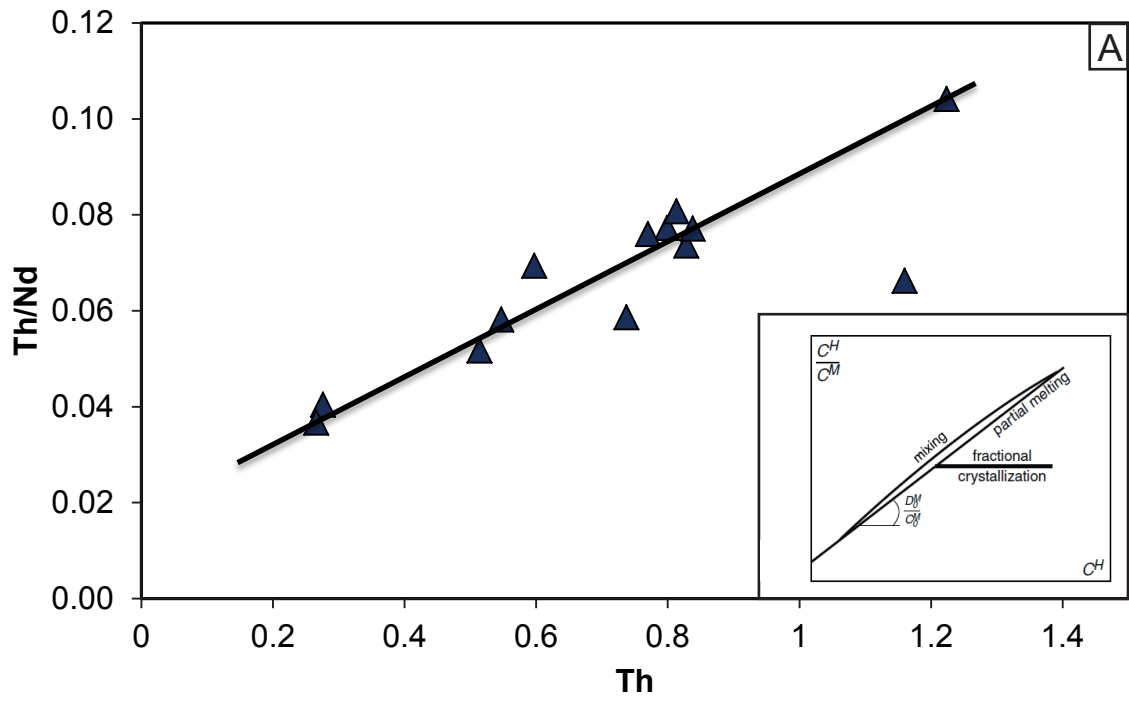


Figure 9. Bellot et al.

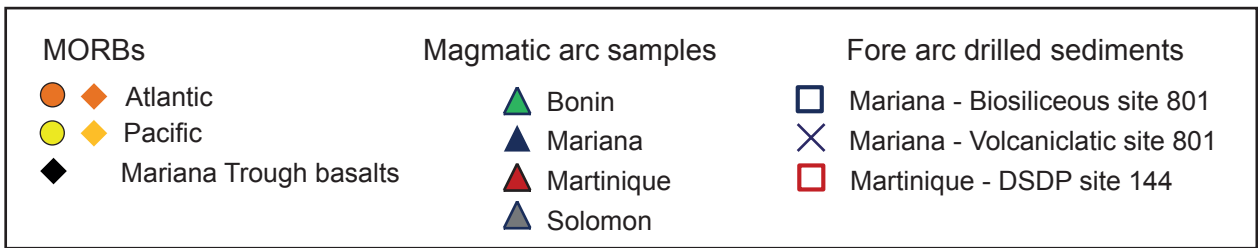
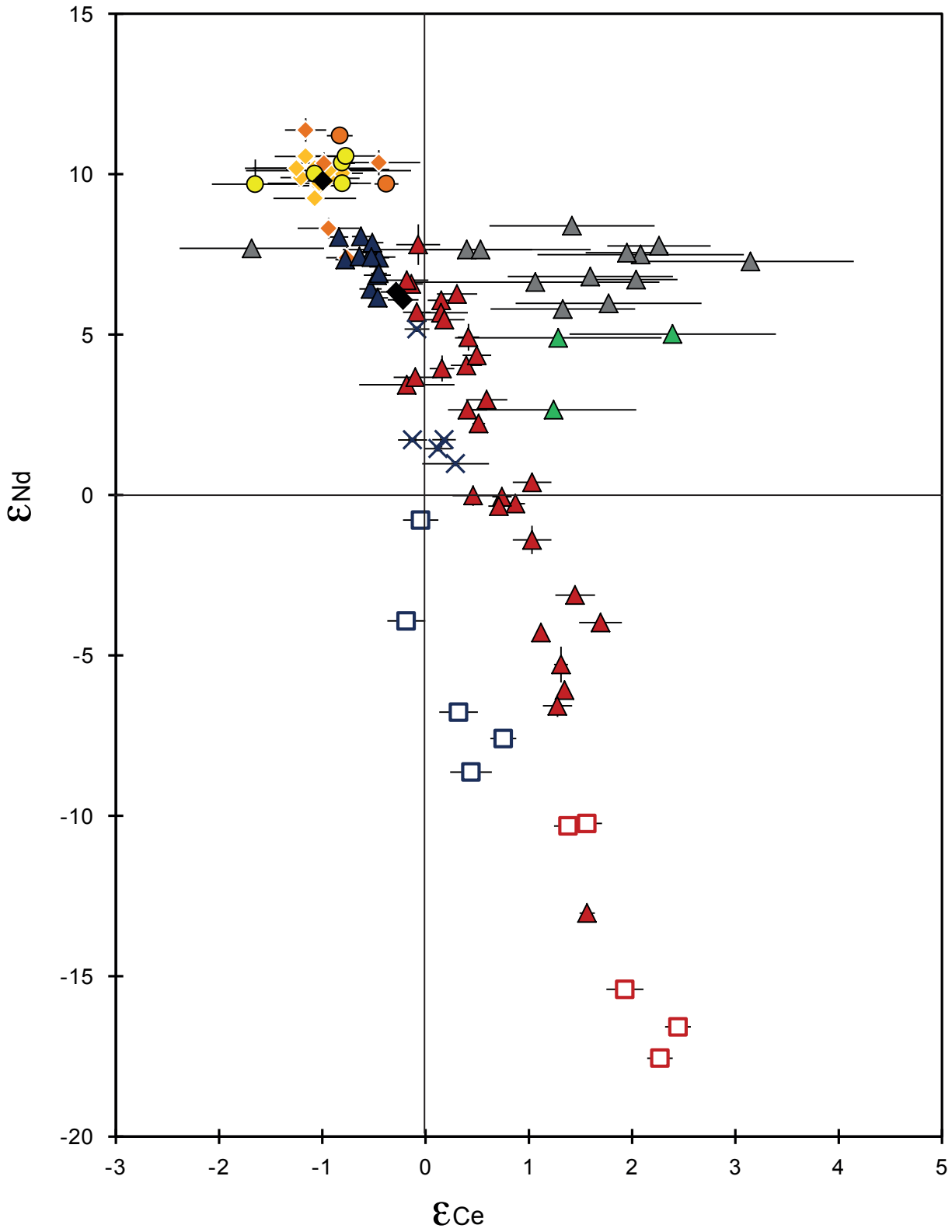


Figure 10. Bellot et al.

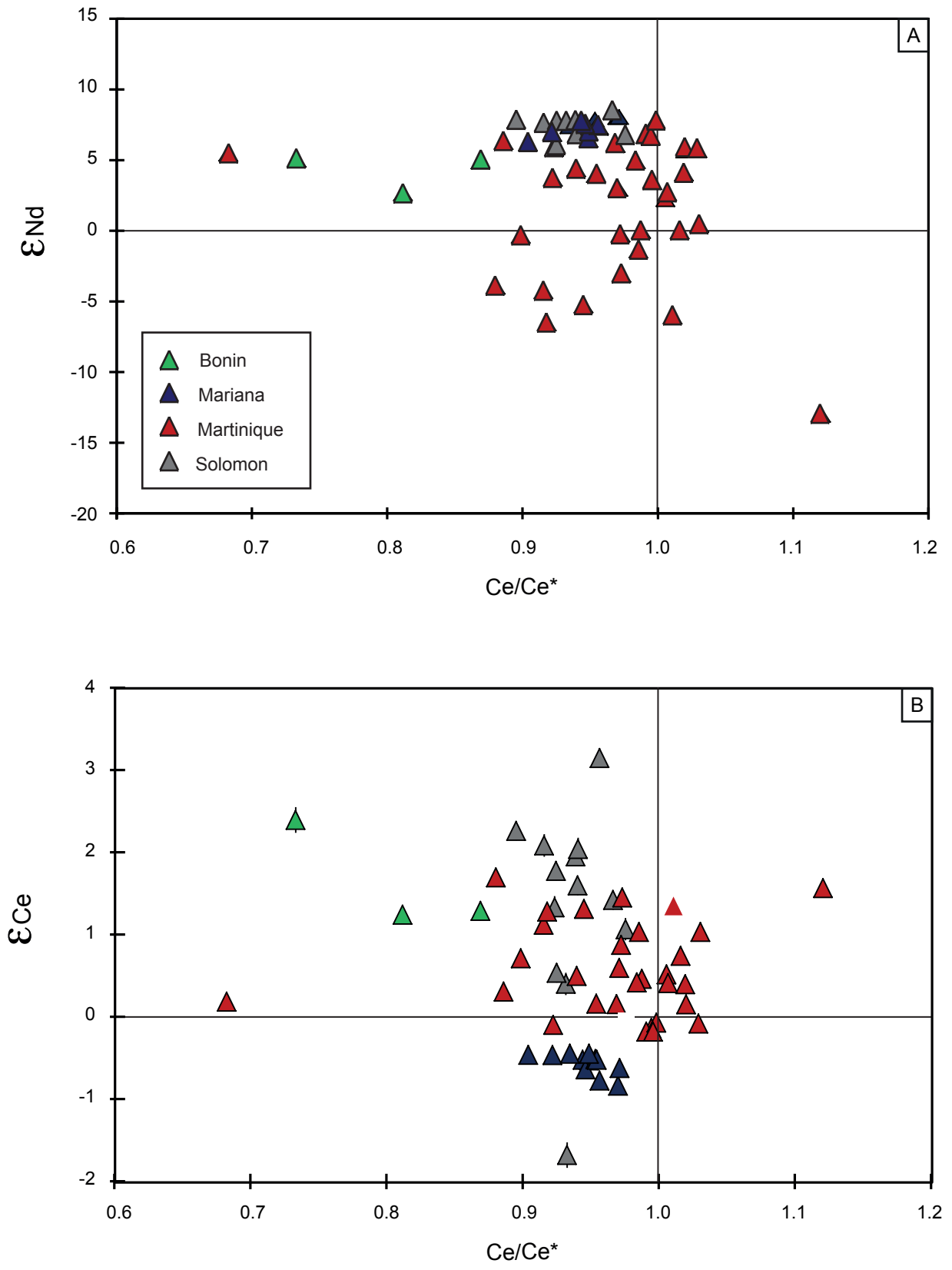


Figure 11. Bellot et al.

Table

[Click here to download Table: table 1.xlsx](#)

			Rare Earth Element concentrations in ppm														
Lavas		SiO ₂ (wt %)	La	Ce	Pr	Nd	Sm	Eu	Gd	Tb	Dy	Ho	Er	Tm	Yb	Lu	
Islands	samples name																
Uracas	URA5	53.6	5.60	12.4	1.77	8.60	2.64	0.97	3.26	0.57	3.77	0.83	2.47	0.36	2.47	0.38	
	URA7	54.2	9.18	19.0	2.55	11.8	3.33	1.18	3.91	0.67	4.29	0.94	2.77	0.41	2.72	0.43	
Asuncion	ASC3	54.5	5.46	12.9	1.97	9.95	3.19	1.15	3.89	0.69	4.40	0.95	2.82	0.43	2.87	0.44	
Agrigan	AGR4a	50.5	7.78	16.3	2.35	10.9	3.01	1.06	3.21	0.54	3.26	0.67	1.97	0.29	1.92	0.29	
Pagan	PAG3	51.6	5.36	12.5	1.89	9.40	2.87	1.04	3.44	0.59	3.72	0.79	2.35	0.34	2.30	0.35	
	MM-92-10	54.5	11.2	24.9	3.68	17.5	5.08	1.65	5.61	0.93	5.91	1.25	3.64	0.53	3.58	0.55	
Alamagan	ALAM2	55	6.27	14.4	2.12	10.3	3.20	0.99	3.72	0.65	4.16	0.90	2.67	0.41	2.71	0.42	
	ALAM5	53.4	6.23	14.1	2.08	10.1	3.09	1.01	3.60	0.63	4.03	0.86	2.55	0.38	2.55	0.39	
Guguan	GUG3	51.6	8.90	18.2	2.67	12.6	3.62	1.29	4.11	0.70	4.38	0.92	2.69	0.40	2.64	0.41	
	GUG6	51.1	3.26	8.3	1.31	6.84	2.30	0.88	2.88	0.51	3.33	0.72	2.13	0.32	2.17	0.33	
	GUG9	51.0	3.46	8.8	1.40	7.26	2.46	0.94	3.10	0.55	3.58	0.78	2.30	0.35	2.32	0.37	
Sarigan	SAG1	53.4	7.44	16.5	2.37	11.3	3.34	1.14	3.77	0.64	4.11	0.88	2.58	0.38	2.57	0.39	
Sediments	Depth (mbsl)	Lithology															
ODP Leg 129 Site 801A	8R-1-1-3-II	Chert	97.9	21.8	26.2	5.37	18.2	3.80	0.91	4.09	0.62	3.57	0.72	1.95	1.73	0.26	
	17R-1-28-30-III	Porcellanite	80.4	17.0	30.1	4.08	14.1	2.83	0.74	2.73	0.42	2.20	0.41	1.11	1.00	0.15	
ODP Leg 129 Site 801B	12R-1-64-70-II	Porcellanite	77.4	10.7	22.4	2.88	12.4	2.85	0.87	3.58	0.56	3.68	0.78	2.26	2.08	0.32	
	5R-01W-40-42-III	Volc. Turbidite	67.8	16.4	32.0	4.44	18.4	3.82	1.10	3.60	0.59	2.86	0.50	1.29	1.04	0.14	
	7R-01W-35-37-III	Volc. Turbidite	50.9	20.0	38.5	5.15	20.9	4.11	1.18	3.64	0.61	3.06	0.56	1.47	1.29	0.19	
	8R3-115-125-III	Volc. Turbidite	257	19.7	41.4	5.54	21.6	4.52	1.42	4.27	0.66	3.39	0.62	1.59	1.32	0.19	
	25R-1-49-53-IV	Radiolarite	86.1	11.8	19.3	2.95	9.96	2.04	0.45	1.94	0.31	1.71	0.34	0.95	0.97	0.15	
	33R-1-143-150-IV	Radiolarite	74.0	21.0	32.7	4.96	18.8	3.76	1.35	3.29	0.49	2.65	0.49	1.34	1.29	0.20	
ODP Leg 129 Site 802A	19R-1-27-29- II	nannofossils+ Volc. Glass	45	20.8	50.8	6.52	29.0	7.15	2.37	7.42	1.11	6.33	1.16	2.98	0.38	2.33	0.32
	43R-03W-33-35-V	Volc. Turbidite	385.43	23.8	45.6	6.53	27.2	5.81	1.78	5.42	0.76	4.34	0.79	2.05	0.27	1.65	0.21
Mariana Trough Basalts	Segment																
C7-DREDGE-3	SSP			9.98	18.7	2.58	11.7	3.13	1.06	3.54	0.55	3.48	0.73	2.12	0.31	2.08	0.31
	D3-2-1	SSP	50.4	9.11	17.5	2.60	11.8	3.12	1.07	3.49	0.54	3.50	0.73	2.11	0.31	2.08	0.31
	D68-2-1	SMT-16	50.8	3.28	9.91	1.74	9.30	3.14	1.18	4.24	0.71	4.77	1.01	2.94	0.42	2.74	0.40
Pacific MORB	Latitude	Longitude															
Searise 1 DR05	02°28'N	102°30'W	50.7	4.43	13.6	2.52	13.9	4.84	1.65	6.90	1.17	8.07	1.72	5.02	0.73	4.82	0.71
Cyana CY82	12°43'N	103°92'W		8.94	22.8	3.33	15.8	4.23	1.56	4.99	0.91	5.77	1.22	3.44		3.24	0.49
Clipperton DR01	12°45'N	103°56'W	46.7	4.20	11.8	1.98	10.5	3.37	1.22	4.37	0.79	5.24	1.12	3.27		3.06	0.45

Table 1

Table
[Click here to download Table: table 2.xlsx](#)

Ce Analytical session		$^{138}\text{Ce}/^{142}\text{Ce}$	2 s.e.	ϵ_{Ce}	2 s.e.	$^{138}\text{Ce}/^{142}\text{Ce}$ average	ϵ_{Ce} average	$^{143}\text{Nd}/^{144}\text{Nd}$	2 s.e.	ϵ_{Nd}	2 s.e.
Lavas											
URA-5	1	0.02256410	0.00000030	-0.57	0.13	0.02256422	-0.52	0.513010	0.000003	7.40	0.06
	1	0.02256579	0.00000112	0.17	0.50						
URA-7	1	0.02256440	0.00000027	-0.44	0.12	0.02256438	-0.45	0.512980	0.000003	6.82	0.05
	1	0.02256435	0.00000036	-0.47	0.16						
ASC-3	1	0.02256457	0.00000028	-0.37	0.12	0.02256424	-0.52	0.513035	0.000002	7.90	0.05
	1	0.02256357	0.00000039	-0.81	0.17						
AGR-4a	1	0.02256434	0.00000030	-0.47	0.13			0.512983	0.000003	6.89	0.06
PAG-3	1	0.02256408	0.00000025	-0.59	0.11	0.02256395	-0.64	0.513017	0.000003	7.55	0.05
	1	0.02256383	0.00000025	-0.70	0.11						
MM92-10	1	0.02256438	0.00000022	-0.45	0.10			0.513011	0.000003	7.43	0.06
ALAM-2	1	0.02256316	0.00000032	-0.99	0.14	0.02256365	-0.78	0.513021	0.000003	7.63	0.05
	1	0.02256408	0.00000030	-0.59	0.13						
ALAM-5	1	0.02256457	0.00000028	-0.37	0.12	0.02256422	-0.52	0.513001	0.000003	7.24	0.05
	1	0.02256391	0.00000026	-0.66	0.11						
GUG-3	1	0.02256359	0.00000036	-0.80	0.16	0.02256436	-0.46	0.512938	0.000003	6.01	0.05
	1	0.02256475	0.00000026	-0.29	0.11						
GUG-6	1	0.02256299	0.00000028	-1.07	0.12	0.02256351	-0.84	0.513041	0.000003	8.02	0.05
	1	0.02256411	0.00000030	-0.57	0.13						
GUG-9	1	0.02256368	0.00000028	-0.76	0.13	0.02256399	-0.62	0.513044	0.000003	8.07	0.05
	1	0.02256430	0.00000028	-0.49	0.12						
SAG-1	1	0.02256420	0.00000024	-0.53	0.11			0.512966	0.000003	6.55	0.05
Sediments											
801A-8R (BS)	2	0.02256743	0.00000042	0.90	0.19			0.512283	0.000003	-6.77	0.06
801A-17R (BS)	2	0.02256665	0.00000042	0.55	0.18	0.02256608	0.30	0.512429	0.000003	-3.93	0.07
	2	0.02256551	0.00000041	0.05	0.18						
801B-12R (BS)	2	0.02256645	0.00000039	0.47	0.17			0.512590	0.000004	-0.79	0.07
801B-5R (Volc)	4	0.02256580	0.00000026	0.18	0.11			0.512718	0.000003	1.72	0.05
801B-7R (Volc)	4	0.02256511	0.00000032	-0.13	0.14			0.512718	0.000003	1.71	0.05
801B-8R3 (Volc)	4	0.02256605	0.00000073	0.29	0.32			0.512680	0.000003	0.97	0.06
801B-25R (BS)	2	0.02256792	0.00000035	1.12	0.15			0.512187	0.000003	-8.64	0.07
801B-33R (BS)	2	0.02256809	0.00000028	1.19	0.12	0.02256800	1.15	0.512241	0.000003	-7.60	0.06
	2	0.02256716	0.00000042	0.78	0.19						
	2	0.02256831	0.00000029	1.29	0.13						
802A-19R (Volc)	4	0.02256521	0.00000027	-0.08	0.12			0.512895	0.000003	5.17	0.06
802A-43R (Volc)	4	0.02256567	0.00000030	0.12	0.13			0.512704	0.000003	1.44	0.06
Back-arc basalts (MTB)											
C7-Dredge-3	3	0.02256513	0.00000029	-0.12	0.13	0.02256491	-0.22	0.512942	0.000002	6.08	0.05
	3	0.02256461	0.00000034	-0.35	0.15						
D3-2-1	3	0.02256532	0.00000035	-0.03	0.15	0.02256476	-0.28	0.512954	0.000002	6.33	0.04
	3	0.02256421	0.00000034	-0.53	0.15						
D68-2-1	2	0.02256375	0.00000036	-0.73	0.16	0.02256315	-1.00	0.513132	0.000003	9.79	0.06
	3	0.02256195	0.00000052	-1.53	0.23						
Pacific MORB											
Searise 1 DR05	3	0.02256365	0.00000068	-0.77	0.30			0.513171	0.000003	10.56	0.05
Cyana CY82	3	0.02256168	0.00000095	-1.65	0.42			0.513127	0.000002	9.69	0.05
Clipperton DR01	3	0.02256358	0.00000034	-0.81	0.15			0.513128	0.000003	9.71	0.05

Table 2

Table

[Click here to download Table: table 3.xlsx](#)

	La	Ce	Pr	Nd		experimental conditions	
Enrichment factor ^a	0.4	0.3	0.3	0.2	<i>Johnson & Plank (1999)</i>	2GPa-800°C	
Enrichment factor ^a	1.4	1.4	1.3	1.1	<i>Martindale et al. (2013)</i>	3GPa-850°C	
	[La] ppm	[Ce] ppm	[Pr] ppm	[Nd] ppm	Ce/Ce*	Eps Ce	Eps Nd
Depleted end-member	0.265	0.773	0.131	0.713	1.00	-1.00	9.79
BS sediment (801B-33R) derived end-member	16.4	26.1	4.00	14.7	0.78	1.15	-7.60
BS sediment (801A-17R) derived end-member	16.4	26.1	4.00	14.7	0.88	0.30	-3.93
VC sediment (801B-7R) derived end-member	20.0	39.4	5.40	22.0	0.93	-0.13	1.71
VC sediment (801B-8R3) derived end-member	20.0	39.4	5.40	22.0	0.97	0.29	0.97

Table 3

Background dataset for online publication only

[Click here to download Background dataset for online publication only: Supp file A.pdf](#)

Background dataset for online publication only

[Click here to download Background dataset for online publication only: Supp file B.pdf](#)

Background dataset for online publication only

[Click here to download Background dataset for online publication only: Supp file C.pdf](#)

Background dataset for online publication only

[Click here to download Background dataset for online publication only: Supp file D.pdf](#)

Background dataset for online publication only

[Click here to download Background dataset for online publication only: Supp file E.pdf](#)

Background dataset for online publication only

[Click here to download Background dataset for online publication only: Supp file F.pdf](#)

Background dataset for online publication only

[Click here to download Background dataset for online publication only: Supp file G.pdf](#)